Physics – Uspekhi **44** (8) 785 – 811 (2001)

REVIEWS OF TOPICAL PROBLEMS PACS numbers: **61.66.–f**, 61.72.Ji, **63.20.–e**

Effect of isotopic composition on phonon modes. Static atomic displacements in crystals

A P Zhernov, A V Inyushkin

DOI: 10.1070/PU2001v044n08ABEH000965

Contents

Abstract. Theoretical and experimental work relevant to isotopic (mass) effects in solids is reviewed. The effect of isotopic composition on the phonon spectrum is discussed with particular emphasis on chemically pure and nearly perfect semiconductor single crystals. The fundamental role of polarization vectors in polyatomic compounds is pointed out. Static atomic displacements around isotopic impurities — an effect potentially leading to considerable phonon (and electron) scattering in strongly anharmonic crystals — are also discussed.

1. Introduction

The characteristic properties of a chemical element are determined by the charge of its nucleus. Most elements possess a certain 'primary group' composed of isotopes. The isotopes of a given element are chemically identical and, in general, they are also the same physically, with the exception of those properties that depend directly on the atomic mass. The isotopes may be stable or they may exhibit natural radioactivity. There are also man-made (unstable) radioactive isotopes. As far as stable isotopes are concerned, 21 chemical elements occur in only one configuration of protons and neutrons (with the exception of beryllium, they all have an odd number of protons). All other elements have from two to ten stable isotopes. The isotope abundance in different groups varies considerably (Table 1).

Many solids are composed of elements that have two or more stable isotopes. The physical properties of solids to some extent depend on the isotopic composition. As a rule, the isotopic effects are relatively weak. In some cases, however, the properties may vary in a considerable and even dramatic way.

The first experimental studies of isotope effects in solids date back to the 1930s. In 1935, Ubbelohde [2] noticed that

A P Zhernov Institute of Superconductivity and Solid State Physics, Russian Research Centre 'Kurchatov Institute', pl. Kurchatova 1, 123182 Moscow, Russian Federation
Tel. (7-095) 196-91 48. E-mail: zhernov@mail.ru
A V Inyushkin Institute of Molecular Physics, Russian Research Centre 'Kurchatov Institute', pl. Kurchatova 1, 123182 Moscow, Russian Federation
Tel. (7-095) 196-74 28. Fax (7-095) 194-19 94
E-mail: inyushkin@imp.kiae.ru

Received 14 March 2001, revised 21 May 2001
Uspekhi Fizicheskikh Nauk **171** (8) 827 – 854 (2001)
Translated by A S Dobroslavskiĭ; edited by A Radzig

Table 1. Natural isotopic compositions of certain elements [1]. The isotopic abundances are given in at.%.

Isotope	f_i	Isotope	f_i	Isotope	f_i	Isotope	f_i
^{1}H	99.985	^{27}Al	100	^{66}Zn	27.9	^{75}As	100
^{2}H	0.015			^{67}Zn	4.1		
		^{28}Si	92.23	^{68}Zn	18.8	^{106}Cd	1.25
^{6} Li	7.5	^{29}Si	4.67	^{70}Zn	0.6	^{108}Cd	0.89
^{7}Li	92.5	^{30}Si	3.10			^{110}Cd	12.49
				^{69}Ga	60.108	^{111}Cd	12.80
^{10}B	19.9	^{31}P	100	^{71}Ga	39.892	^{112}Cd	24.13
^{11}B	80.1					^{113}Cd	12.22
		^{32}S	95.02	^{70}Ge	21.23	^{114}Cd	28.73
^{12}C	98.90	^{33}S	0.75	^{72}Ge	27.66	^{116}Cd	7.49
^{13}C	1.10	^{34}S	4.21	^{73}Ge	7.73		
		^{36}S	0.02	^{74}Ge	35.94	^{112}Sn	0.97
^{14}N	99.634			^{76}Ge	7.44	^{114}Sn	0.65
^{15}N	0.366	^{35}Cl	75.77			^{115}Sn	0.34
		^{37}Cl	24.23	^{74}Se	0.89	^{116}Sn	14.53
^{16}O	99.762			^{76}Se	9.36	^{117}Sn	7.68
^{17}O	0.038	^{63}Cu	69.17	^{77}Se	7.63	^{118}Sn	24.23
^{18}O	0.200	^{65}Cu	30.83	^{78}Se	23.78	^{119}Sn	8.59
				^{80}Se	49.61	^{120}Sn	32.59
^{19}F	100	^{64}Zn	48.6	^{82}Se	8.73	^{122}Sn	4.63
						^{124}Sn	5.79

the replacement of one isotope in a solid with another alters the vibrational and rotational spectra of molecules, but has no significant effect on the structure of the interatomic potential. Naturally, given the limited accuracy of measurements and scarceness of the stable isotopes within the researcher's reach, the first studies used the most accessible isotopes of hydrogen — ^{1}H and ^{2}H (deuterium) — mainly in complex hydrogen compounds, such as water, ammonia, ammonium halides, metal hydrides, organic and other compounds. Mainly studied were the isotope effects on the structural properties. The isotopic composition was found to affect the geometry of chemical bonds [1] and the phase transition temperatures (in the case of polymorphous transformations and ferroelectric phase transitions).

The rapid progress of nuclear science and technology (including the technology of large-scale isotope separation) for military applications during and after World War II led in particular to the accumulation of stable isotopes of both light and heavy elements in quantities sufficient for carrying out experiments with simple compounds. In 1950s, such remarkable effects were discovered as the isotopic shift of the superconducting transition critical temperature of mercury [4, 5] and a considerable (severalfold) increase in the thermal conductivity of isotopically enriched germanium crystal [6]. The first of these effects was the key clue for Bardeen, Cooper and Schrieffer [7] in their construction of the microscopic theory of low-temperature superconductivity in 1957. Thus, 46 years after the discovery of superconductivity in mercury by H Kamerlingh-Onnes, one of the most difficult problems in solid-state physics was finally solved. At the same time, the isotopic effect on the thermal conductivity of germanium, which very clearly demonstrated how strong the effect of *isotopic crystal lattice disordering* can be, supported the theory of Pomeranchuk [8] formulated as early as 1942. According to his theory, it is the random isotope distribution over the lattice that restricts the increase of thermal conductivity of dielectric crystals at low temperatures. The exceptionally high thermal conductivity of isotopically pure crystals shows promise for adaptation to technology dealing with high thermal loads — for example, in diamond monochromators for synchrotron radiation or in microelectronics.

In subsequent years, systematic studies of isotopic effects were performed with hydrides and deuterides, quantum crystals, solutions of quantum liquids and crystals of ^{3}He and ^{4}He. The investigations into other solid compounds were, as a rule, incidental.

Hydrides and deuterides are heavily used in modern technology, for example, in nuclear engineering as heat-resistant moderators, for separation and storage of hydrogen isotopes, in powder metallurgy, and in the chemical industry as catalysts. Hydrides and deuterides are a unique and peculiar object of physical studies. Isotopic substitution in such systems considerably alters the electronic and phonon spectra, as well as the magnetic and superconducting properties. The bulk of research has been done for hydrides and deuterides of the transition and rare-earth metals. A review of the experimental and theoretical works can be found, for example, in monograph [9].

The conductivity and superconductivity of weak hydrides and deuterides of s – p-metals have also been studied experimentally. Such compounds are obtained by forced saturation of metals with hydrogen and deuterium. In the theoretical aspect, these systems attracted a certain interest. The reason is that atomic hydrogen in a metal loses its electron: the proton is localized in the interstitial position, and the electron is collectivized. The structure of the resulting impurity is ultimately simple. As a result, weak hydrides make up simple model systems, very convenient for theoretical speculations (see, for example, monograph [10]).

Finally, it is well known that in sufficiently perfect transition metals the hydrogen and deuterium atoms, together with the mu-meson, are localized near the gaseous impurities and migrate in a subbarrier way between adjacent interstitial sites. Such tunneling atoms make up a typical quantum-mechanical two-level system. In this case the characteristic parameter of the problem — the difference in energy between antisymmetric and symmetric states in the 'well' — by virtue of the Gamow factor exhibits an exponential dependence on the mass of the light particle as $\sqrt{M}$. Because of this, the properties associated with tunneling show a strong dependence on the isotopic composition. The situation is more complicated in metals where electron screening of the tunneling particle takes place. For reviews of this problem the reader is referred to monograph [11] and papers [12 – 15].

Bose and Fermi excitation branches coexist in ^{3}He – ^{4}He systems. Commonly used here is the technique for obtaining extra low temperatures by diluting ^{3}He in ^{4}He. The physical properties of ^{3}He – ^{4}He systems have been discussed in a number of reviews and monographs (see, for example, Refs [16, 17]).

There is also a vast body of scientific literature on isotope effects for the case of quantum crystals. Here we want to mention the works of the Moscow group of I G Sadikov and S N Ishmaev [18 – 20], and the Khar'kov group of V G Manzheliĭ [21 – 24].

Attention is drawn to the fact that crystals composed of several isotopes of a given element are a particular case of crystals with impurities. Because of this, the methods and ideas developed for slightly imperfect systems are readily adapted to problems that relate to isotopically disordered crystals. The foundations of the dynamical theory of crystal lattices with impurity atoms were laid down in the works of A A Maradudin and E Montroll [25, 26] in the West, and I M Lifshitz and Yu M Kagan [27 – 29] in Russia. They studied many features of the impurity deformation of the phonon spectrum and their effects on various properties of crystals. Today's views on the dynamics of systems involving impurities have much benefited from the work of the experimental group of N A Chernoplekov from the Russian Research Centre 'Kurchatov Institute' (Moscow) (see the review in book [10]). Many issues of isotopic alloys and crystals with impurities have a common nature.

To obtain reliable experimental data it is necessary to compare samples that are identical in chemical composition and structure, and only differ in the isotopic composition. A very important experimental problem is the presence of uncontrollable impurities in the samples that may disguise the isotopic effects under investigation. In the optimal situation, which often is very difficult to realize, the concentration of chemical impurities and lattice defects is made so low that their effects are much weaker than the isotopic effects.

Great advances in the technology of fabricating ultrapure materials (primarily semiconductors) and the reorientation of the isotope production industry to peaceful purposes

[1] Such effects became known as Ubbelohde effects [3].

after the end of the cold war in the late 1980s together allowed the production of unique chemically and isotopically pure, nearly defect-free (perfect) massive single crystals of simple substances — diamond, germanium and silicon — that are of considerable interest for the industry. Diamond crystals with different isotopic composition were grown in the laboratory of the General Electric Co. (USA) [30, 31] (several millimeters across, and a few carats in mass m), and crystals of germanium ($\sim$ 15 cm in length, $\sim$ 1 cm^2 in cross section, and $m \sim 100$ g in mass) were the result of joint efforts of the Institute of Molecular Physics of the Russian Research Centre 'Kurchatov Institute' (Moscow) and the Lawrence National Laboratory in Berkeley (USA) [32]. There are recent reports on the production of isotopically enriched silicon crystals (ranging from 1 to 10 grams) in the international cooperation of scientists from Russia, Germany and Japan [33–35]. Photographs of these unique crystals are shown in Figs 1–3. Observe that the growth of these semiconductor crystals and other crystals whose isotopic content is different from natural is a quite formidable task, because it is necessary to carry out chemical purification of a small quantity of the initial isotope preparation and prevent 'isotopic contamination' of the material at every stage of the crystal growth that usually takes place at high temperatures [36].

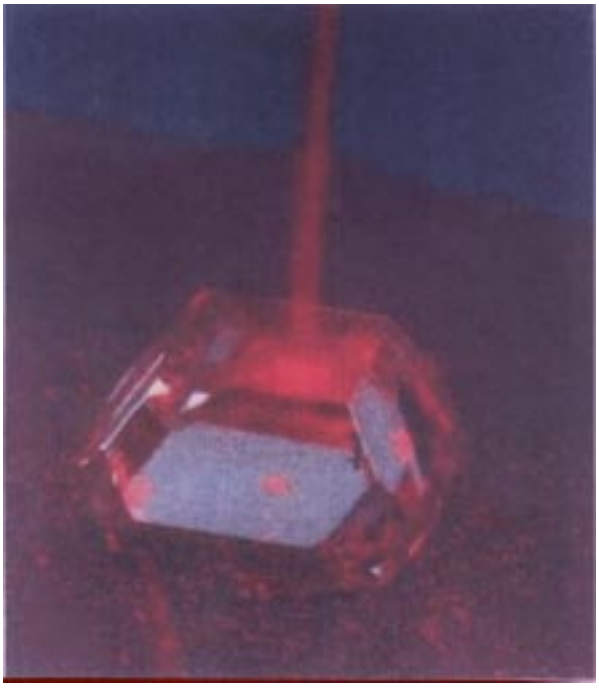

Figure 1. Isotopically modified 1.2-ct diamond containing 99.5% of ^{13}C [by courtesy of *Sci. News* **138** 5 (1990)].

It is interesting that such properties of synthetic isotopically pure ^{12}C diamond as the exceptionally low fluorescence in the visible spectrum (about an order of magnitude lower than in natural diamonds), high purity and structural perfection make it a practically ideal material for diamond anvils in superhigh-pressure devices for spectroscopic studies [37].

In this review we consider the isotopic effects in solids due to the different *masses* of isotopes, based on recent theoretical and experimental results. The main attention is paid to the analytical treatment of recent experiments with semiconductor materials. The latter were used for carrying out complex theoretical and experimental studies of the phonon and electronic spectra, structural properties and the kinetic coefficients. Left beyond the scope of this review are the interesting isotopic effects in oxide materials (cuprates, manganites, nickelates, titanates, etc.), fullerenes, borides and the like. We do not consider lattice excitations associated with the rotational degrees of freedom of atoms. Neither do we discuss the physical phenomena related to the differences in other characteristics of isotopes, such as, for example, the magnetic and quadrupole moments of nuclei, neutron absorption and scattering cross sections.

Figure 2. Single crystal of an isotopically pure (99.99%) germanium isotope ^{70}Ge.

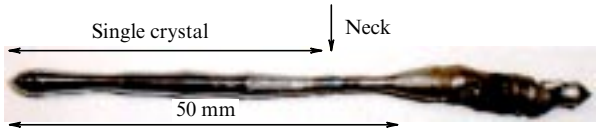

Figure 3. Single crystal of an isotopically pure (over 99.9%) silicon isotope ^{28}Si [34].

In solids, the parameters of the interatomic force interaction practically do not depend on the isotope composition because the configuration of the atomic electron shell is very weakly correlated with the nuclear mass: the scale of this effect is on the order of the electron mass to the nuclear mass ratio, $m_e/M \sim 10^{-4}$. The dependence on the isotopic composition arises because the motion of an atom in the potential created by surrounding atoms depends, among other things, on its mass. Vibrations of atoms at the lattice points may be regarded as their motion in the harmonic potential whose parameters depend on the volume of the crystal unit cell — the *quasi-harmonic approximation*. Then the frequency and the square of the amplitude of atomic vibrations are proportional to $M^{-1/2}$.

Isotope ('mass') effects are usually divided into two types. The first relates the properties of the solid to the average mass M_c of an atom of each constituent chemical element ($M_c = \sum_i c_i M_i$, where c_i and M_i are the concentration and the mass of the ith isotope). The second type refers to the dependence of solid properties on the degree of isotopic disorder. In practically all solids (with the exception of solid helium at low temperatures), the isotopes are generally distributed in the lattice at random, and the measure of isotopic disorder is given by

$$\xi^2 = \sum_i c_i \left(\frac{\Delta M_i}{M_c} \right)^2 , \quad \Delta M_i = M_i - M_c .$$

Such effects are not present in isotopically pure and isotopically ordered solids.

Polyatomic lattices involving elements of considerably different masses open up interesting additional possibilities. In such lattices, the isotopic composition can be varied for both light and heavy elements. As it turns out, this will considerably modify the frequencies for certain phonon branches in certain regions of the Brillouin zone, thus leading to renormalization of the associated parameters. Secondly, in such a situation the crystal is dynamically disordered with respect to one sublattice, while remaining regular for the other sublattice. This fact, for example, allows direct investigation into the effects of elastic scattering of phonon modes, attributable to isotopic disorder and related to particular components of the compounds.

A direct manifestation of the effects of isotopic composition on the properties of the solid is the isotopic deformation of the phonon spectrum. It should be emphasized that to a first approximation the real crystal in which the isotopes are randomly distributed over lattice sites may be considered using the *virtual crystal model*. This model does not explicitly take into account the isotopic disorder. It is assumed that the masses of atoms in the unit cell are equal to the *average arithmetic masses* for the particular composition of isotopes [38, 45]. Then for a monatomic crystal the isotopic frequency shift $\Delta\omega$ is inversely proportional to $\sqrt{M_c}$. For a polyatomic lattice, the shift $\Delta\omega$ is additionally proportional to square of the modulus of the corresponding polarization vector. We see that even in the linear approximation with respect to the isotope mass difference, the isotopic effects are directly visible in the phonon spectrum, and indirectly through the electron–phonon interaction in the electronic spectrum. In the quasiharmonic approach, one can also assess the effects of the isotopic composition on the temperature dependence of the lattice constant and the elastic moduli. It turns out that the parameters of materials with different isotopic compositions are linked by *universal* relationships.

To the second-order approximation with respect to the parameter ξ^2 of mass fluctuation, the anharmonic renormalizations are supplemented by additional contributions to damping Γ and frequency shift $\Delta\omega$ of the phonon modes. Recently such effects were studied for a number of crystals using Raman and IR spectroscopy. For the frequencies of optical phonons, deviations were observed from the linear mass dependence as the isotopic composition was varied. These experimental findings cannot be interpreted within the virtual crystal approximation: one has to use a more realistic model of lattice dynamics — for example, the *coherent potential approximation* (a version of the mean field theory) [40–42] or the *supercell method* [10, 43–45]. The recursion method [46–48] is efficient when one needs to find the one-particle Green function (formed on the operators of dynamic atomic displacements) averaged over the impurity configurations.

In this review the isotopic effects in the phonon spectra are discussed in Section 2.

In crystals with isotopic disorder, the mean square of dynamic atomic displacements $\langle u^2 \rangle$ (with respect to equilibrium positions) is not the same when we move from one unit cell to another. Such *dynamic disordering* even to the first order with respect to ΔM gives rise to fields of static displacements (deformations) of the lattice near the 'impurity' isotopes that break the local symmetry of the lattice. Static displacements also modify the local force parameters. The superposition of random fields induced by static displacements near the isotopes gives rise to a fluctuating component in the interatomic distances in crystals, which may be considerable even for traditional crystals.

We call attention to the fact that when the nucleus displays an electric quadrupole moment, the chaotic distribution of the crystal electric field may downgrade the symmetry of the electric field from the side of the environment of the nucleus and lead to splitting of the set of nuclear energy levels. The study of NMR spectra in this situation may, in principle, reveal the particular configurations of the fields of static displacements and their temperature dependences. Such studies have recently been performed with germanium crystals. The issues related to the static displacements of the lattice atoms near the isotopic impurity are discussed in Section 3.

In the immediate future we are planning to discuss the effects of isotopic disorder on the kinetic coefficients of semiconductors and metals. Of great importance are also the results of investigations into the isotopic effects on the structural properties of single crystals and on their electronic spectrum.

2. Phonon modes

As noted above, variation of the isotope composition in the crystal lattice may give rise to effects of first and second order with respect to the isotope mass difference ΔM. Here we discuss the theoretical and experimental results related to the appropriate renormalizations in the spectra of phonon modes. First we appeal to the virtual crystal approximation to analyze the isotopic frequency shift for polyatomic and monatomic compounds. Then we consider the effects of isotopic disorder (an effect proportional to $\sim \Delta M^2$) on the lifetimes and frequencies of the phonon modes. Theoretical evaluations are made in the framework of perturbation theory using the instrument Green functions; we also rely on the coherent potential method and the supercell method. We pay attention to the strong dependence of the parameters of isotopically disordered systems on the polarization vectors of the phonon modes. The theoretical part ends with a brief summary of the phenomenological models available for the ion-covalent-bonded crystals, and the schemes of phonon spectrum calculations from first principles.

As regards the experimental material, we discuss the most recent optical measurements with monatomic and diatomic semiconductors. In the case of monatomic systems, we analyze the results for the Raman one-phonon spectra, and for the Raman and IR two-phonon spectra. Effects linear and quadratic in ΔM are clearly identifiable in these spectra. Positively established for diatomic compounds is the depen-

dence of the isotopic frequency shift on the modulus squared of the corresponding polarization vector. Concrete models of the dynamic interatomic interaction are therewith verified, and we also discuss the anomalous behavior of transverse optical (TO) phonons, observed in the Raman spectra of GaP and CuCl. This behavior is interpreted as a manifestation of Fermi resonance (the anharmonic type of interaction of a TO-phonon with a biphonon). Analysis of the TO-spectrum distortion caused by the variation of isotopic composition allows one to identify the individual contributions of modes associated with the atoms of compound components in a particular anharmonic process.

2.1 Isotopic shift of phonon frequencies in a polyatomic crystal

In this section we discuss the isotopic frequency shift of the vibrational mode in a crystal whose unit cell contains atoms of different elements. The mean values of atomic masses are used for the elements. The masses of the isotopes of the same element are assumed to be close to each other. We consider the effect linear with respect to the isotope mass difference — that is, our treatment is confined to the virtual crystal approximation. In this approximation, the point symmetry group of the crystal lattice generally speaking remains unchanged — as a consequence, the vibrational spectrum does not change, and the degeneracy is not removed. In reality, in a crystal lattice with isotopic disorder there appear fields of static atomic displacements because the zero-point oscillations of various isotopes are different (see Section 3). With the exception of the case of quantum crystals, however, the static atomic displacements are very small compared with the distance between the atoms. This allows us to disregard them in the present context.

2.1.1 Isotopic frequency shift. Let us reproduce here the main equations of the dynamical theory of regular crystals (see, for example, Refs [26, 38, 49, 50]). Consider the crystal lattice of N unit cells, each of which in the general case contains r atoms of different elements. The cells are numbered with a subscript $\mathbf{n}$, and the positions of atoms within the cell are numbered with a superscript k. The dynamic matrix $\Phi^{(c)}_{\alpha\alpha'}(kk'|\mathbf{q})$ of a virtual crystal is defined by a relationship of the type

$$\Phi^{(c)}_{\alpha\alpha'}(kk'|\mathbf{q}) = \frac{1}{N}\,\frac{1}{\sqrt{M_c^{(k)}M_c^{(k')}}} \times \sum_{\mathbf{n}\mathbf{n}'} \varphi_{\alpha\alpha'}(\mathbf{n}k,\mathbf{n}'k')\exp\left[i\mathbf{q}(\mathbf{R}^{(0)}_{\mathbf{n}}-\mathbf{R}^{(0)}_{\mathbf{n}'})\right]. \quad (2.1)$$

Here, $\varphi_{\alpha\alpha'}(\mathbf{n}k,\mathbf{n}'k')$ is the matrix of the second-order force parameters, and α, α' are the Cartesian indices. The average atomic mass of an element k taken over an isotopic composition c is

$$M_c^{(k)} = \sum_i c_i^k M_i^{(k)}. \quad (2.2)$$

In addition, $\mathbf{R}^{(0)}_{\mathbf{n}}$ is the vector of the equilibrium position of the $\mathbf{n}$th unit cell. The dynamic matrix is a Hermitian matrix of $3s\times 3s$ dimension — that is, the following equality holds:

$$\Phi^{(c)}_{\alpha\alpha'}(kk'|\mathbf{q}) = \Phi^{*(c)}_{\alpha'\alpha}(k'k|\mathbf{q}). \quad (2.3)$$

The eigenvectors $\mathbf{e}^{(c)}(k|l)$ (or the polarization vectors) and the eigenvalues $\omega(l)$ of this matrix satisfy the equation

$$\omega^2(l)e^{(c)}_\alpha(k|l) = \sum_{k',\alpha'}\Phi^{(c)}_{\alpha\alpha'}(kk'|\mathbf{q})e^{(c)}_{\alpha'}(k'|l), \quad (2.4)$$

where the index l is the aggregate $\{\mathbf{q}\,j\}$ of the wave vector $\mathbf{q}$ and the polarization index $j\,(1\leqslant j\leqslant 3r)$ for the lth vibrational mode. Because $\Phi(\mathbf{q})$ is Hermitian, the polarization vectors satisfy the conditions of orthonormality and completeness of the form

$$\sum_{k,\alpha} e^{*(c)}_\alpha(k|\,\mathbf{q}\,j)e^{(c)}_\alpha(k|\,\mathbf{q}\,j') = \delta_{jj'}, \quad (2.5a)$$

$$\sum_{j} e^{*(c)}_\alpha(k|\,\mathbf{q}\,j)e^{(c)}_{\alpha'}(k'|\,\mathbf{q}\,j) = \delta_{kk'}\delta_{\alpha\alpha'}. \quad (2.5b)$$

As is well known, the calculation of an eigenvalue, correct to a certain order of magnitude with respect to perturbation, requires knowledge of the eigenfunctions up to the nearest lower order. Accordingly, when the isotopic composition is varied over the component k_1, the change of the eigenvalue (the square of frequency) in the first approximation is equal to the corresponding diagonal element of the perturbation energy, taken with respect to the unperturbed states (see, for example, Refs [51, 52]). We have then

$$\left(\frac{\Delta\omega^2(l)}{\Delta M^{(k_1)}}\right)_c = \sum_{k,\alpha}\sum_{k',\alpha'} e^{*(c)}_\alpha(k|l)\left(\frac{\Delta\Phi^{(c)}_{\alpha\alpha'}(kk'|\mathbf{q})}{\Delta M^{(k_1)}}\right)_c e^{(c)}_{\alpha'}(k'|l). \quad (2.6)$$

Using the definition of the dynamic matrix (2.1), it is easy to find that

$$\left(\frac{\Delta\Phi^{(c)}_{\alpha\alpha'}(kk'|\mathbf{q})}{\Delta M^{(k_1)}}\right)_c = -\frac{1}{2}\Phi^{(c)}_{\alpha\alpha'}(kk'|\mathbf{q})\left[\frac{\delta_{kk_1}}{M_c^{(k)}}+\frac{\delta_{k_1k'}}{M_c^{(k')}}\right]. \quad (2.7)$$

Now we substitute expression (2.7) into equation (2.6). Since the change of the average mass, generally speaking, proceeds continuously, we may replace the difference Δ with the differentiation sign, and get

$$\frac{d\ln\omega_c^2(l)}{d\ln M_c^{(k)}} = -\sum_\alpha \left|e^{(c)}_\alpha(k|\,l)\right|^2. \quad (2.8a)$$

From the last equation we immediately see that in a polyatomic crystal the frequency shift of the vibrational mode, caused by the change of the average atomic mass of one of the compound elements, is proportional to the modulus squared of the appropriate polarization vector. In the case of a monatomic crystal, when the lattice unit cell contains atoms of one and the same element, in place of Eqn (2.8a) we have

$$\frac{d\ln\omega_c^2(l)}{d\ln M_c} = -1. \quad (2.8b)$$

Equations (2.8a) and (2.8b) constitute the basic equations of the virtual crystal model. To the best of our knowledge, these equations were first put forward in work [53] dealing with the effects of isotopic composition on the properties of fullerenes.

Notice that relations (2.8) give direct information about the polarization vectors of phonons, if their frequencies and isotopic frequency shifts are known from experiment. This allows them to be used in the analysis of the efficiency of various dynamic models descriptive of the force interactions between the atoms.

2.1.2. Model of a two-atom linear chain. Let us consider the example of a linear chain of atoms of two different elements with masses $M^{(1)}$ and $M^{(2)}$ ($M^{(1)} \geqslant M^{(2)}$), which occupy alternating positions. Assume that the dynamic forces only act between the adjacent atoms. With such a lattice, the vibrational spectrum has two branches: acoustical ($j = 1$), and optical ($j = 2$). Their frequencies $\omega(l)$ and the squares of the polarization vectors $\left|\mathbf{e}(k|l)\right|^2$ are given by the following formulas

$$\omega^2(qj) = \omega_0^2\left[1 - \epsilon_{1j}\,\phi(q)\right], \quad \omega_0^2 = \frac{\gamma}{\mu}, \tag{2.9a}$$

$$\phi(q) = \left(1 - \frac{4M^{(2)}/M^{(1)}}{\left(1 + M^{(2)}/M^{(1)}\right)^2}\sin^2 qa\right)^{1/2}, \tag{2.9b}$$

$$\left|\mathbf{e}(k|qj)\right|^2 = \frac{1}{2}\left(1 + \epsilon_{1k}\epsilon_{1j}\,\frac{1 - M^{(2)}/M^{(1)}}{1 + M^{(2)}/M^{(1)}}\,\frac{1}{\phi(q)}\right). \tag{2.10}$$

Here, a is the lattice constant, γ is the effective force parameter, and μ is the reduced mass:

$$\mu = \frac{M^{(1)}M^{(2)}}{M^{(1)} + M^{(2)}}. \tag{2.11a}$$

In the above equations, the symbol q denotes the wave vector:

$$q = \frac{\pi\eta}{a}, \quad -\frac{1}{2} \leqslant \eta \leqslant \frac{1}{2}. \tag{2.11b}$$

The function $\epsilon_{1k(j)} = 1$ if $k(j) = 1$, and $\epsilon_{1k(j)} = -1$ if $k(j) \neq 1$.

The following relations hold for the model in question, with due account for Eqn (2.10):

$$\left|\mathbf{e}(1|q1)\right|^2 = \left|\mathbf{e}(2|q2)\right|^2, \quad \left|\mathbf{e}(1|q2)\right|^2 = \left|\mathbf{e}(2|q1)\right|^2. \tag{2.12}$$

Besides, on the upper spectrum edge at $q_b = \pi/2a$ we have

$$\left|\mathbf{e}(k|q_b j)\right|^2 = \frac{1}{2}\left(1 + \epsilon_{1k}\epsilon_{1j}\right). \tag{2.13}$$

From equations (2.12) it follows that the complete behavior pattern of $\left|\mathbf{e}(k|l)\right|^2$ is established if one has an opportunity to analyze the moduli squared of polarization vectors for only one atom.

Let us first consider the situation when the masses of atoms in the unit cell are drastically different: $M^{(1)} \gg M^{(2)}$. As follows from relations (2.9)–(2.12), the square of polarization vector $|\mathbf{e}(2|q2)|^2$ corresponding to the vibrations of a light atom in the optical range exhibits a weak dependence on the wave vector and is close to 1. For the heavy atom, however, the modulus squared of the polarization vector is close to 1 within the band of the acoustic lattice vibrations ($k, j = 1$). At the same time, $|\mathbf{e}(2|q1)|^2$ and $|\mathbf{e}(1|q2)|^2$ are much less than 1. This is a reflection of the fact that the light atom vibrates mainly on the optical branches, and the heavy atom on the acoustic branches.

In the general case, when the atomic mass difference between the compound components is not large, the value of $|\mathbf{e}(k|l)|^2$ is finite over the entire vibrational spectrum and depends on the wave vector, for which reason the value of the derivative $\mathrm{d}\ln\omega(l)/\mathrm{d}\ln M^{(k)}$ is considerably different from $-1/2$.

To illustrate this conclusion, Fig. 4 shows $\omega^2(l)$ and $|\mathbf{e}(2|l)|^2$ for the light atom as functions of the wave vector and the atomic mass ratio $M^{(1)}/M^{(2)}$.

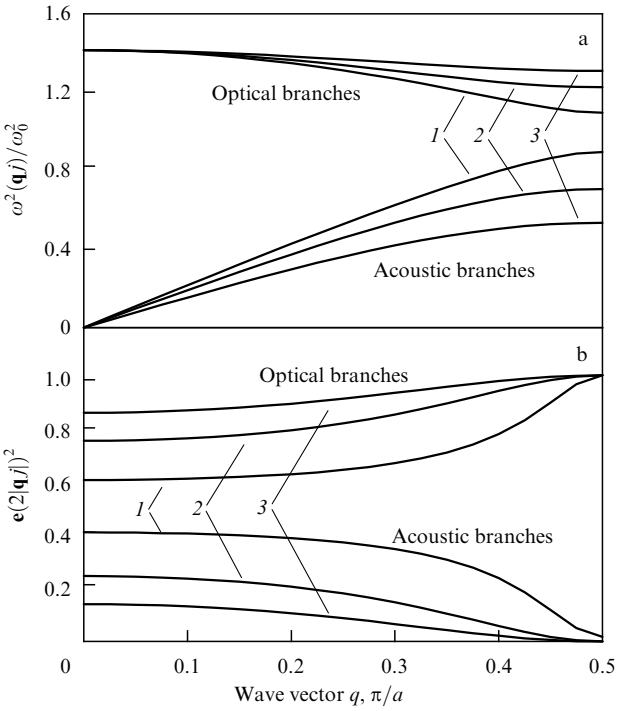

Figure 4. Squares of the frequencies $\omega^2(l)$ and polarization vectors $|\mathbf{e}(2|l)|^2$ for the light atom as functions of the wave vector in the two-atom chain. Curves *1*, *2*, *3* correspond to $M^{(1)}/M^{(2)} = 1.5$, 3 and 6, respectively.

In this way, from formulas (2.9), (2.10) it follows that when the atomic masses of the compound components are essentially different, the partial vibrational spectra of the heavy and light atoms practically do not overlap. If the isotopic composition is varied over one of the components, only the respective partial spectrum is renormalized. When the atomic masses of the compound components are close to each other, then both the partial spectra are varied but in an asymmetrical manner with one changing more strongly than the other.

2.2 Shift and damping of the phonon modes owing to the isotopic disorder

2.2.1 Perturbation theory. Let us now discuss the problem of renormalization and decay of vibrational mode frequencies in a diatomic crystal, caused by isotopic disorder. We will take into account the effects both linear and quadratic with respect to the isotope mass difference in the framework of perturbation theory. For the sake of simplicity we assume that only one element in the compound has several isotopes.

In the harmonic approximation, the crystal lattice vibrations are described by the Hamiltonian

$$H = \sum_{\mathbf{n}k}\frac{(p^{\alpha}_{\mathbf{n}k})^2}{2M^{(k)}_{\mathbf{n}}} + \frac{1}{2}\sum_{\mathbf{n}k,\,\mathbf{n}'k'}\varphi_{\alpha\beta}(\mathbf{n}k,\mathbf{n}'k')u^{\alpha}_{\mathbf{n}k}u^{\beta}_{\mathbf{n}'k'}. \tag{2.14}$$

Here we have used the following notation: $\mathbf{p}_{\mathbf{n}k}$ and $\mathbf{u}_{\mathbf{n}k}$ are the operators of momentum and dynamic displacement of an

atom with the mass $M_{\mathbf{n}}^{(k)}$, occurring at the $\mathbf{n}$th lattice point and occupying the kth position in the cell ($k = 1, 2$), and $\varphi_{\alpha\beta}(\mathbf{n}\,k, \mathbf{n}'k')$ is the second-order force parameter; hereinafter the summation is taken over the twice repeating Cartesian indices α and β. For definiteness, we shall assume that the element having several isotopes occupies position number one ($k = 1$) in the unit cell, and the element with the single isotope occupies position number two ($k = 2$).

The series expansion of the atomic displacement in the lattice in terms of the Bose amplitudes $b_{\mathbf{q}j}$ and $b^*_{\mathbf{q}j}$ is as follows

$$\mathbf{u}_{\mathbf{n}k} = \sum_{\mathbf{q}j} \sqrt{\frac{\hbar}{2NM_{\mathbf{n}}^{(k)}\omega(\mathbf{q}j)}} \Big\{ \mathbf{e}(k|\,\mathbf{q}\,j) \exp[\mathrm{i}\mathbf{q}\mathbf{R}_{\mathbf{n}}^{(0)}]\, b_{\mathbf{q}\,j} + \mathbf{e}^*(k'|\mathbf{q}j) \exp[-\mathrm{i}\mathbf{q}\mathbf{R}_{\mathbf{n}}^{(0)}]\, b^*_{\mathbf{q}\,j} \Big\}, \tag{2.15}$$

where $\mathbf{R}_{\mathbf{n}}^{(0)}$ is the equilibrium position vector of the $\mathbf{n}$th cell. With the help of formula (2.15), the original Hamiltonian can be brought to the diagonal form.

To find the parameters of the phonon modes in the isotopically disordered lattice, we introduce the retarded Green function constructed in terms of operators of the atomic displacements:

$$\widetilde{D}^{\alpha\beta}_{\mathbf{n}\,k,\,\mathbf{n}'k'}(t) = -\mathrm{i}\theta(t) \Big\langle \big[u^{\alpha}_{\mathbf{n}\,k}(t), u^{\beta}_{\mathbf{n}'k'}(0)\big] \Big\rangle . \tag{2.16}$$

From here on, the angle brackets $\langle \ldots \rangle$ denote averaging over the equilibrium thermodynamic distribution.

Making use of the commutation relations for the displacement and momentum operators, one can express the equation of motion for the Green function $\widetilde{D}$ (2.16) in the form

$$-\frac{\mathrm{d}^2}{\mathrm{d}t^2}\, \widetilde{D}^{\alpha\beta}_{\mathbf{n}\,k,\,\mathbf{n}'k'}(t) - \frac{1}{M_{\mathbf{n}}^{(k)}} \sum_{\mathbf{n}_1,\,k_1,\,\gamma} \varphi_{\alpha\gamma}(\mathbf{n}k, \mathbf{n}_1k_1) \widetilde{D}^{\gamma\beta}_{\mathbf{n}_1k_1,\,\mathbf{n}'k'}(t) = \frac{1}{M_{\mathbf{n}}^{(k)}}\, \delta(t)\, \delta_{\alpha\beta}\, \delta_{\mathbf{n}\,k,\,\mathbf{n}'k'} . \tag{2.17}$$

After Fourier transform, equation (2.17) becomes

$$\sum_{\mathbf{n}_1,\,k_1,\,\gamma} \big[\omega^2 M_{\mathbf{n}}^{(k)}\, \delta_{\alpha\gamma}\, \delta_{\mathbf{n}\,\mathbf{n}_1} \delta_{kk_1} - \varphi_{\alpha\gamma}(\mathbf{n}k, \mathbf{n}_1k_1)\big] \widetilde{D}^{\gamma\beta}_{\mathbf{n}_1k_1,\,\mathbf{n}'k'} = \delta_{\alpha\beta}\delta_{\mathbf{n}\,\mathbf{n}'}\delta_{k\,k'} . \tag{2.18}$$

The last equation can be rewritten in the symmetrized form

$$\sum_{\mathbf{n}_1,\,k_1,\,\gamma} \left[\omega^2\delta_{\alpha\gamma}\delta_{\mathbf{n}\mathbf{n}_1}\delta_{kk_1} - \frac{1}{\sqrt{M_{\mathbf{n}}^{(k)} M_{\mathbf{n}_1}^{(k_1)}}}\, \varphi_{\alpha\gamma}(\mathbf{n}k, \mathbf{n}_1k_1)\right] \times \sqrt{M_{\mathbf{n}_1}^{(k_1)} M_{\mathbf{n}'}^{(k')}}\, \widetilde{D}^{\gamma\beta}_{\mathbf{n}_1k_1,\,\mathbf{n}'k'} = \delta_{\alpha\beta}\, \delta_{\mathbf{n}\mathbf{n}'}\delta_{kk'} . \tag{2.19}$$

Observe that the solution $D^{(\mathrm{c})}$ of Eqn (2.19) in the virtual crystal approximation is expressed via the frequencies and polarization vectors of the corresponding dynamic matrix. We have then

$$\widetilde{D}^{(\mathrm{c})\alpha\beta}_{\mathbf{n}\,k,\,\mathbf{n}'k'}(\omega) = \frac{1}{\sqrt{M_{\mathrm{c}}^{(k)} M_{\mathrm{c}}^{(k')}}}\, \frac{1}{N} \sum_{\mathbf{q}\,j} e^{(\mathrm{c})*}_{\alpha}(k|\,\mathbf{q}\,j)\, e^{(\mathrm{c})}_{\beta}(k'|\,\mathbf{q}j) \times \frac{\exp\big[-\mathrm{i}\mathbf{q}(\mathbf{R}_{\mathbf{n}}^{(0)} - \mathbf{R}_{\mathbf{n}'}^{(0)})\big]}{\omega^2 - \omega_{\mathrm{c}}^2(\mathbf{q}j) + \mathrm{i}\delta} = \frac{1}{\sqrt{M_{\mathrm{c}}^{(k)} M_{\mathrm{c}}^{(k')}}}\, D^{(\mathrm{c})\alpha\beta}_{\mathbf{n}\,k,\mathbf{n}'k'}(\omega) . \tag{2.20}$$

The atomic mass of the element that has different isotopes at the position $k = 1$ of the unit cell obeys the equality

$$M_{\mathbf{n}}^{(k)} = M_{\mathrm{c}}^{(k)} + \big(M_{\mathbf{n}}^{(k)} - M_{\mathrm{c}}^{(k)}\big)\delta_{k1} . \tag{2.21}$$

From Eqns (2.18), (2.19) and (2.21) we get the standard equation for the Green function $\tilde{D} = (1/M)D$ introduced in Eqn (2.20):

$$D^{\alpha\beta}_{\mathbf{n}\,k,\,\mathbf{n}'k'}(\omega) = D^{(\mathrm{c})\alpha\beta}_{\mathbf{n}\,k,\,\mathbf{n}'k'}(\omega) + \omega^2 \sum_{\mathbf{n}_1k_1,\,\mathbf{n}_2k_2} D^{(\mathrm{c})\alpha\gamma}_{\mathbf{n}\,k,\,\mathbf{n}_1k_1}(\omega)\, V^{\gamma\gamma_1}_{\mathbf{n}_1k_1,\,\mathbf{n}_2k_2}(\omega) D^{\gamma_1\beta}_{\mathbf{n}_2k_2,\,\mathbf{n}'k'}(\omega) , \tag{2.22}$$

where

$$V^{\alpha\beta}_{\mathbf{n}\,k,\,\mathbf{n}'k'} = \omega^2 \big(M_{\mathrm{c}}^{(k)} - M_{\mathbf{n}}^{(k)}\big)\delta_{\mathbf{n}\mathbf{n}'}\delta_{kk'}\delta_{k1}\delta_{\alpha\beta} . \tag{2.23}$$

Taking advantage of the fact that the masses of the isotopes are close, one can seek an approximate solution of Eqn (2.22) by an iterative procedure. In so doing it is necessary to perform averaging over the isotope distribution. This operation restore the translational symmetry of the crystal lattice. Concrete calculations are done for the spatial Fourier component of the Greenian. The series expansion of D in each order in V involves terms of the type $V^m[\omega^2 - \omega^2(\mathbf{q}j)]^{-(m+1)}$. Let us carry out summation for the pole terms in the series. In the case of a cubic crystal, for the averaged Green function we get

$$\big\langle D^{\alpha\beta}_{\mathbf{n}\,k,\,\mathbf{n}'k'}(\omega)\big\rangle_{\mathrm{c}} = \frac{1}{N} \sum_{\mathbf{q}\,j} \exp\big[-\mathrm{i}\mathbf{q}(\mathbf{R}_{\mathbf{n}}^{(0)} - \mathbf{R}_{\mathbf{n}'}^{(0)})\big] \times e^{(\mathrm{c})*}_{\alpha}(k|\,\mathbf{q}\,j) e^{(\mathrm{c})}_{\beta}(k'|\,\mathbf{q}\,j) \Big[\big(D_{\mathbf{q}}^{(\mathrm{c})}\big)^{-1} - \Pi_{\mathrm{iso}}(\mathbf{q})\Big]^{-1}_{jj'} . \tag{2.24}$$

Here $\langle \ldots \rangle_{\mathrm{c}}$ denotes averaging over the different configurations of the isotopes of the 'first' kind. Then one finds

$$\big(D_{\mathbf{q}}^{(\mathrm{c})}\big)_{jj'} = \delta_{jj'}\big[\omega^2 - \omega_{\mathrm{c}}^2(l)\big]^{-1} . \tag{2.25}$$

Recall that $l \equiv \{\mathbf{q}j\}$. By Π_{iso} we denoted the mass operator associated with the isotopic disorder, which obeys the following relations

$$\Pi_{\mathrm{iso}}(\mathbf{q}jj', \omega) \approx \omega^4(l)\xi^2(k = 1)\, D^{(\mathrm{c})}_{01,01}(\mathbf{q}jj', \omega) , \tag{2.26}$$

$$D^{(\mathrm{c})}_{01,01}(\mathbf{q}jj', \omega) = \sum_{\gamma,\gamma'} e^{(\mathrm{c})}_{\gamma}(1|\,\mathbf{q}\,j) \left(\frac{1}{N} \sum_{l_1} \frac{e^{(\mathrm{c})}_{\gamma}(1|l_1)\, e^{(\mathrm{c})}_{\gamma'}(1|l_1)}{\omega^2 - \omega_{\mathrm{c}}^2(l_1) + \mathrm{i}\delta}\right) e^{(\mathrm{c})}_{\gamma'}(1|\,\mathbf{q}\,j') . \tag{2.27}$$

The frequency shift $\Delta_{\mathrm{iso}}(l, \omega)$ of the phonon mode and its decay $\Gamma_{\mathrm{iso}}(l, \omega)$ due to the elastic scattering by the mass fluctuations with the rate $\tau^{-1}_{\mathrm{iso}}(l, \omega)$ are expressed via the real and imaginary parts of the mass operator Π_{iso}:

$$\frac{\Pi_{\mathrm{iso}}(l, \omega)}{2\omega} = \Delta_{\mathrm{iso}}(l, \omega) + \mathrm{i}\,\frac{1}{2}\,\Gamma_{\mathrm{iso}}(l, \omega) , \tag{2.28}$$

$$\Delta_{\mathrm{iso}}(l, \omega) = \frac{\pi}{6}\, \omega_{\mathrm{c}}^3(l) \sum_{k} \xi^2(k) \big|\,\mathbf{e}^{(\mathrm{c})}(k|l)\big|^2\, \frac{1}{\pi} \int_0^{\omega_m} \mathrm{d}\omega'\, \frac{\rho_k(\omega')}{\omega^2 - \omega'^2}\, \delta_{k,1} , \tag{2.29}$$

$$\Gamma_{\rm iso}(l,\omega) = \tau_{\rm iso}^{-1}(l,\omega) = \frac{\pi}{6}\,\omega_{\rm c}^2(l)\sum_k \xi^2(k)\left|\mathbf{e}^{(\rm c)}(k|l)\right|^2\rho_k(\omega)\delta_{k,1}\,, \quad (2.30)$$

where $\rho_k(\omega)$ is the partial density of the phonon states for the atoms of the kth sublattice:

$$\rho_k(\omega) = \frac{1}{3N}\sum_l \left|\mathbf{e}^{(\rm c)}(k|l)\right|^2\delta\left[\omega-\omega_{\rm c}(l)\right]. \quad (2.31)$$

From equations (2.29), (2.30) we directly see that in the polyatomic compounds, as opposed to the monatomic ones, the shift and damping of the phonon mode under the isotopic substitution depend both on the frequency and on the polarization vectors. It should be emphasized that the dependence on the polarization vectors is very strong, because

$$\Delta_{\rm iso} \quad \text{and} \quad \Gamma_{\rm iso} \sim \left|\mathbf{e}^{(\rm c)}(k|l)\right|^4.$$

In the case of monatomic compounds, from Eqns (2.29) – (2.31) we find the standard formulas for the frequency shift and damping of the phonon modes that do not depend on the polarization vectors:

$$\Delta_{\rm iso}(l,\omega) = \frac{\pi}{6}\,\omega_{\rm c}^3(l)\xi^2\,\frac{1}{\pi}\int_0^{\omega_m} {\rm d}\omega'\,\frac{\rho(\omega')}{\omega^2-\omega'^2}\,, \quad (2.32)$$

$$\Gamma_{\rm iso}(l,\omega) = \frac{\pi}{6}\,\omega_{\rm c}^2(l)\xi^2\rho(\omega)\,, \quad (2.33)$$

$$\rho(\omega) = \frac{1}{6N}\sum_l \delta\left[\omega-\omega_{\rm c}(l)\right]. \quad (2.34)$$

It is interesting to note that, by contrast to the monatomic compounds, for the polyatomic compounds with considerably different masses of components, by varying the isotopic composition over one of the components, one can effectively control the lifetime of vibrational modes in either the acoustical or optical ranges of the phonon spectrum. In this way it is possible, for example, to dramatically change the thermal conductivity at either low or high temperatures.

An expression of the type (2.30) for $\tau_{\rm iso}^{-1}$ has been derived in different ways (see, for example, monograph [26]). Tamura [54] inferred the expression for $\tau_{\rm iso}^{-1}$ up to the fourth order with respect to the isotope mass difference.

Notice that for the different models of interatomic force interaction the phonon frequencies in the symmetrical directions are, as a rule, practically the same. *At the same time, unlike the frequencies* $\omega(\mathbf{q}j)$*, the polarization vectors* $\mathbf{e}(k|\,\mathbf{q}j)$ *in such models can behave quite differently*. (In particular, this implies that the definition of the model parameters of the force interaction between the atoms requires complete knowledge of the phonon spectrum — that is, one needs to know both $\omega(\mathbf{q}j)$ and $\mathbf{e}(k|\,\mathbf{q}j)$.) Because of this, in the case of polyatomic crystals the pulse dependences of $\tau_{\rm iso}^{-1}$, especially in the short wave range of the spectrum, are in principle very sensitive to the nature of the interatomic interaction. This can be illustrated with the results produced by Tamura [55], where Eqn (2.30) was turned to account for the quantitative analysis of the peculiar patterns of the acoustic mode relaxation times for the diatomic crystals GaAs and InSb. The phonon modes were described using the deformable dipole model [56 – 59] and a version of the shell model [60 – 62]. In both models of the interatomic force interaction, the frequency spectra are in fairly good agreement between themselves and with the experimental findings (Fig. 5), while the polarization vectors are considerably different (Fig. 6). The profound effect of the interatomic interaction on the frequency dependence of the isotopic scattering time $\tau_{\rm iso}$ in the case of GaAs is illustrated in Fig. 7.

The shell model [63 – 66] implies that the ions with the intertialess charged shell, bound by elastic forces, reside at the lattice sites. By assumption, each ion interacts both with the adjacent ions and with their shells. Pair interactions between

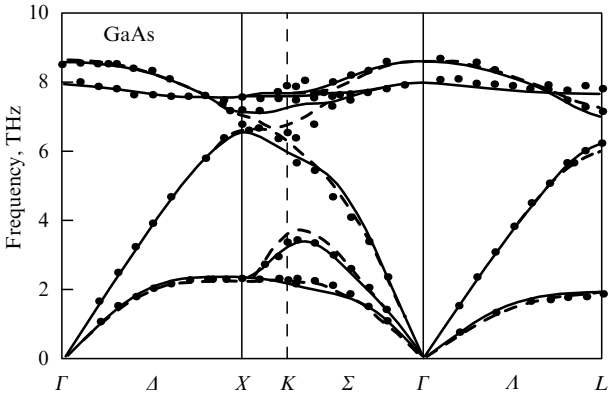

Figure 5. Dispersion curves in GaAs for the three principal directions, constructed using the calculated results for the deformable dipole model (solid lines) and the shell model (dashed lines). The points denote experimental data [55].

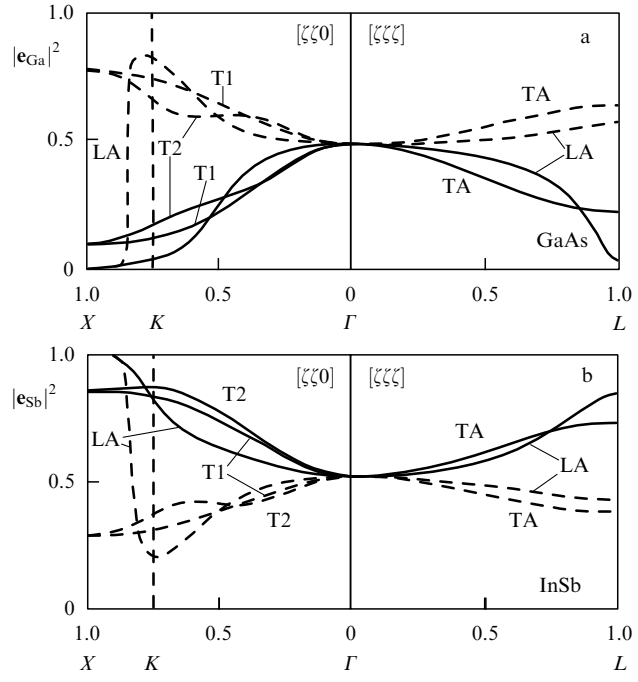

Figure 6. Amplitudes squared of Ga (a) and Sb (b) atomic vibrations as functions of the reduced wave vector in the directions [ζζ0] and [ζζζ]. The solid and dashed lines correspond to the deformable dipole and shell models, respectively. T1 and T2 are the lower and the upper transverse acoustic modes [55].

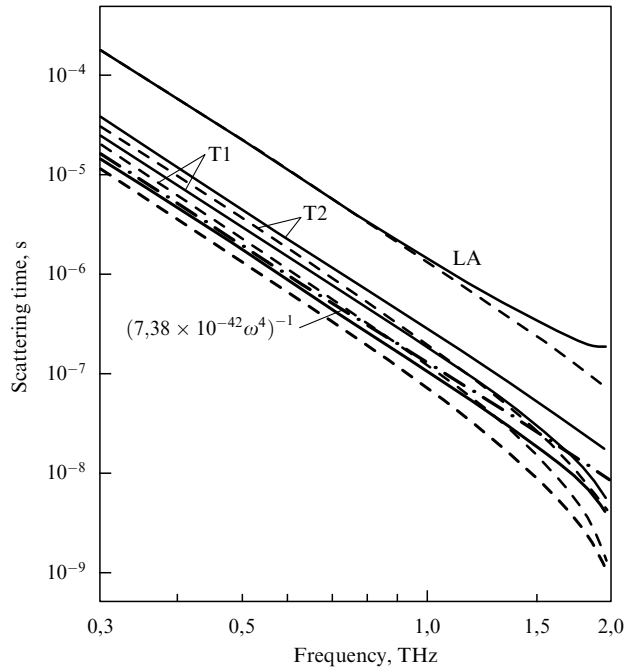

Figure 7. Frequency dependence of the scattering time τ_{iso} of TA-phonons with a vector $\mathbf{q}\|[\zeta\zeta\zeta]$ in GaAs. The solid and dashed lines correspond to the deformable dipole and shell models, respectively. The lines T1, T2 and LA show the contributions to the relaxation time from phonon scattering to each acoustic branch. The dot-and-dash line is the extrapolation of the low-frequency portion, proportional to ω^{-4} [55].

the electron shells of adjacent ions are also taken into account. In this model, concrete mechanisms are proposed for describing the polarizability and mutual deformability of ions. As a matter of fact, what is considered is the adiabatic motion of the electron density with respect to the atoms. In principle, the shell model takes into account the many-particle interionic interaction. In addition to the short-range non-Coulomb and the long-range Coulomb interactions, the deformable dipole model takes detailed account of the lattice polarization. Then the dipole moment of the crystal is determined by three contributions that arise because of the displacement of the ion equilibrium charge, the action of the electric field of the lattice on the ion, and the ion deformation by the Coulomb type forces. Unlike the shell model, the deformable dipole model only takes into consideration some part of the short-range interactions. Both these models were widely utilized in the 1970s. Currently, the bond-charge model is often used as the phenomenological model (see Section 2.2.3 and Appendix).

One of the present authors (A P Zh) dealt with the description of force parameters for the anisotropic diatomic metal zinc [67, 68], using complete [knowledge of $\omega(\mathbf{q}j)$ and $\mathbf{e}(k|\mathbf{q}j)$] and incomplete [knowledge of only $\omega(\mathbf{q}j)$] experimental data on the phonon spectrum. In particular, the shape of the microcontact spectra of the electron–phonon interaction in Zn single crystals depending on the orientation of the microbridge with respect to the crystallographic axes was analyzed. By definition, these spectra exhibit a significant dependence on the polarization vectors $\mathbf{e}(k|\mathbf{q}j)$ [69].

2.2.2 Coherent potential and supercell methods. *Coherent potential method.* It is well known that in the theory of crystal lattices with impurities the standard methods of series expansion of the scattering matrix in terms of the concentration of the scattering centers do not work well when the concentration is large. The main reason is that the configuration-averaged expressions are not symmetrical with respect to the replacement of the matrix atom by the impurity atom. Proper relations can be obtained by the *coherent potential method.* This method is a version of the mean field theory, similar to the molecular theory of field in magnetism or the chaotic phase approximation used in the description of the Coulomb interaction between the electrons. It has been described in a number of monographs and reviews (see, for example, Refs [10, 40–42].

Let us find in the framework of the coherent potential approximation the one-particle Green function with due account for multiple scattering. Its mass operator is found in a self-consistent way from the condition that the scattering T-matrix attributed to isotopic disorder is, on average, equal to zero. It is important that this theory allows the diagram technique to be used, thus giving a better understanding of which scattering processes were taken into account and which were neglected.

We confine ourselves to the most simplified assumption that the states at one lattice site do not depend on the other sites in the effective medium. This is the so-called single-site approximation, and it should be applicable to isotopic alloys as long as the static distortion of the crystal lattice can be neglected. Observe that the effective medium is described by the complex eigenvalues whose imaginary part characterizes the lifetime of the single-particle states.

In the single-site approximation in the monatomic crystal lattice, the mass operator is given by an expression of the form (see, for example, Ref. [41])

$$\Pi_{\mathrm{CPA}}(\omega) = \widetilde{\Pi}(\omega) = \sum_i \frac{c_i \epsilon_i \omega^2}{1 - [\epsilon_i \omega^2 - \widetilde{\Pi}(\omega)] D(\omega)}\,, \quad (2.35)$$

where

$$D(\omega) = \frac{1}{N}\sum_l \frac{1}{\omega^2 - \omega_c^2(l) - \widetilde{\Pi}(\omega)}\,, \quad \epsilon_i = 1 - \frac{M_i}{M_c}\,, \quad (2.36)$$

i is the number of an atomic position, and M_i is the mass of the appropriate isotope. Note that in Eqns (2.35) and (2.36) we have made corrections for the multiple occupation of lattice sites (thus precluding the possibility of one site being occupied by two or more isotopes). By replacing the zero Green function $D^{(0)}$ with the complete function D in Eqn (2.35), we took into account the embedded one-site diagrams.

The expression for the imaginary part of the Green function that explicitly includes the frequency shift and damping of the phonon mode is given by

$$\operatorname{Im} D(l,\omega) = \frac{1}{\pi} \operatorname{Im} \frac{1}{\omega^2 - \omega_c^2(l) - \widetilde{\Pi}(\omega)}\,, \quad (2.37)$$

with

$$\widetilde{\Delta}(\omega) = \frac{1}{2\omega} \operatorname{Re} \widetilde{\Pi}(\omega), \quad \widetilde{\gamma}(\omega) = \frac{1}{2\omega} \operatorname{Im} \widetilde{\Pi}(\omega)\,. \quad (2.38)$$

It should be noticed that the coherent potential method has been extended to the many-site approximation (see, for example, Refs [70–72]). In principle, this approximation is suitable for describing the local ordering effects in solid solutions.

Supercell method. According to this method, the crystal is divided into extended cells. The sites of an extended cell contain N_c^3 atoms, and its unit cell holds N_c atoms. This effective cell is employed for constructing the dynamic matrix of the crystal, using the data about the force parameters that describe the interatomic interaction. The eigenfrequencies and eigenvectors are found by diagonalizing the dynamic matrix of the supercells. To find the spectrum of the disordered system, one has to do calculations for all potentially feasible impurity configurations in the extended cell. Such a procedure gives the distribution of the phonon state number for the given vector $\mathbf{q}$ — that is, the imaginary part of the Green function for the phonon mode $\mathbf{q}$.

The method is essentially based on the fact that the phonon spectrum is effectively *self-averaged* when the number of particles is large, i.e. the ensemble distribution of a random quantity for a particular system is the same as that for the ensemble with the same statistical structure (see, for example, Refs [10, 46, 47, 73, 74]).

The effects of the isotopic composition on the phonon spectrum present the simplest case of violation of the crystal lattice translation invariance because of disordering. In the case of isotopes, the disorder does not affect the interatomic interaction which can thus be treated with a high degree of accuracy on the basis of approaches developed for regular crystals. One only has to take account of the existence of an atomic distribution with respect to their masses in the dynamic matrix. This approach is exact in the framework of the harmonic theory.

Observe that the concepts of frequency shift Δ_{iso} and mode damping Γ_{iso} are pertinent to the perturbation theory. The quantities Δ_{iso} and Γ_{iso} represent corrections to the spectrum. They arise because of the elastic phonon – phonon interaction brought about by the 'mass' defects. On the other hand, in the supercell method we 'simply' diagonalize the dynamic matrix, and the arising phonon states have zero width. In this situation, the phonon shift and broadening arise because of the spread of $3N_c$ eigenvalues obtained for each particular isotope distribution. In other words, the finite widths and shifts of spectral distributions are associated here with the realizations of discrete state distributions which are averaged over the numerous distributions of isotopes.

Of the three approaches used for the description of isotopic effects in the phonon spectra of crystals, the most accurate and consistent is the purely numerical supercell method. Perturbation theory is better suited for concrete calculations in the qualitative treatment. It should be emphasized that all approaches give quantitatively similar results, when the disorder parameter $\xi^2 \ll 1$.

2.2.3 Phonons in ion-covalent-bonded crystals. Rapid progress is currently being achieved in the 'first-principle' theory of phonon spectra, developed in the framework of the method of the density functional. In the first place, this approach is based on the exact microscopic expressions for the dynamic matrix of force parameters (see Refs [75, 76] and review [77]). Then the problem reduces to finding the matrix of microscopic electron susceptibility $\chi(\mathbf{q}+\mathbf{B}, \mathbf{q}+\mathbf{B}')$. Observe that the initial equations pertain to the system of 'bare ions plus all electrons'. In real calculations, generally speaking, the contribution from the core electrons is included in the electron interaction energy. In this case the density $\rho(r)$ of nonuniform gas is determined by the valence electron distribution function. Dielectric screening and variational linear response methods were developed for the direct determination of the χ-susceptibility matrix. The dielectric screening method involves straightforward calculation of the static permittivity $\varepsilon(\mathbf{q}+\mathbf{B}, \mathbf{q}+\mathbf{B}')$. This requires solving a Kohn – Sham type equation with local pseudopotentials, and finding the one-electron eigenfunctions and energy values. The dynamic matrix therewith contains a factor ε^{-1}, and the main difficulties are associated with the inversion of high-dimension ε^{-1}-matrices.

We emphasize that the macroscopic electric field exists in ion-covalent-bonded crystals. Because of the existence of such a field, the theory makes use of the effective Born charges Z_k^*. These charges are expressed in terms of the nondiagonal elements of the matrix ε^{-1}:

$$Z_k^* = -\frac{\Omega}{4\pi e^2} \lim_{\mathbf{q}\to 0} \Sigma_{\mathbf{B}} \frac{\varepsilon^{-1}(\mathbf{q}, \mathbf{q}+\mathbf{B})}{\varepsilon^{-1}(\mathbf{q}, \mathbf{q})} \mathbf{q}(\mathbf{q}+\mathbf{B})\, V_k(\mathbf{q}+\mathbf{B})\,. \tag{2.39}$$

According to the known acoustic rule of sums [78], the master dynamic equation for eigenfrequencies and polarization vectors has three solutions ($j = 1, 2, 3$) for $\mathbf{q} \to 0$ with the frequencies $\omega_j(\mathbf{q}) \to 0$. One can demonstrate that this rule is satisfied if the condition of electrical neutrality in the form $\sum_k Z_k^* = 0$ holds for the unit cell. In his way, the nondiagonal elements of the matrix ε^{-1} must be taken into account as a matter of principle in compounds with polar bonds, since this will ensure the local electrical neutrality of the compound and the existence of acoustic branches.

The situation with the application of a variational theory of linear response to finding the electron contribution to the force parameters is as follows. In the first place, a methodical approach known as the Hellmann – Feynman theorem [79, 80] is efficient in calculating the derivatives of energy with respect to the displacements u (the theorem is actually formulated so that it is possible to differentiate the desired function with respect to any variable parameter; in Ref. [81], the theorem was extended to the case of third-order derivatives). Then the force parameters are calculated at once by the perturbation theory [82, 83]. Namely, when the displacements u are small enough, the increments of the eigenfunction, $\Delta\Psi_{n\mathbf{k}}$, and energy, $\Delta\epsilon_{n\mathbf{k}}$, which enter the one-electron Kohn – Sham equation, are linear functions of u. It was found that one can deduce a linear differential equation in $\Delta\Psi_{n\mathbf{k}}$ and the increment ΔV_{eff} of the pseudopotential. The quantity ΔV_{eff} is then expressed via the increment of the electron density $\Delta\rho$ — that is, via $\Delta\Psi_{n\mathbf{k}}$. It is important that these equations only describe the occupied valence states, whereas the electron-free states are not involved explicitly. This theory was developed for the case when the effective pseudopotential includes the sum of the norm-conserving ionic pseudopotentials, and the wave function Ψ is defined as a plane-wave expansion (see the review [77]). A modified variational method was developed by Savrasov [84], where the formalism of MT-orbitals is used. Now let us sum up what has been said so far. The variational theory of linear response allows one to calculate the frequencies and polarization vectors of phonons for arbitrary values of wave vectors without the need for inverting a high-dimension matrix of dielectric constant.

The direct method of 'frozen-in' phonons, based on the direct comparison of energies attributed to the equilibrium and deformed systems, has also been developed and widely used. It is important that for the deformed crystal (with the

frozen normal vibration $l = \{\mathbf{q}j\}$) its effective unit cell (because of the lowered symmetry) is much bigger in size than the analogous cell in the equilibrium crystal. A straightforward self-consistent procedure of energy calculations is only possible for the wave vectors of modes $\mathbf{q}$ commensurate with the reciprocal lattice vectors (in the symmetrical directions [85–88]). A modification of this method by introducing the one-electron reduced density matrix (in the context of perturbation theory) made the calculations much easier [89]. The linear response of the system to an external force is found in a self-consistent way by solving the set of equations that involve the values for the equilibrium crystal with nondisplaced ions. In this case there is no need to find the matrix of electron susceptibility χ. It is also possible to do calculations with nonlocal pseudopotentials. We emphasize that the frozen-in phonon method allows us to analyze the contributions from different microscopic interactions to the formation of particular vibrational modes.

Such a method of calculating the phonon spectra from first principles, based on the formalism of a matrix of microscopic permittivity in the context of self-consistent perturbation theory for a linear response as applied to covalent semiconductors and semiconducting III–V compounds with weak ionicity has been detailed in Refs [90, 91]. In doing so, not only the phonon dispersion curves, but also such dynamic parameters as elasticity moduli, partial Grüneisen parameters, thermal expansion coefficients, etc. were analyzed. We ought also to mention here the work [92] dealing with the detailed experimental (neutron diffractometry) and theoretical analysis of the polarization vector behavior for silicon. In semiconducting II–VI compounds, the energies of cation d-electrons are about 10 eV less than those of s-electrons. Such d-electrons form a weakly disperse band whose energy is higher than for the anion s-band. As a result, the d-electrons have a considerable effect on the shaping of the valence band. The theory has been extended to the case of such systems by Corso et al. [93]. We would also like to mention studies concerned with the dynamic properties of the physically interesting and technically promising materials GaN [94], SiC [95], and CuCl [96].

Along with the calculations from the first principles, phenomenological models are actively used for the analysis of phonon spectra as well. These include the rigid ion model, shell type models (including the proper shell model, the overlapping valence shell model, and the 'breathing' shell model), the deformable dipole model (see, for example, monograph [97], review [98], and overview [99]), and finally the bond-charge (BC) model. In the Appendix, we use the BC model for defining the dynamic matrix for diatomic compounds, and give a summary of the parameter values for many semiconductor crystals. The six-parameter BC model and probably the shell model involving 14 parameters are physically sensible and give a very satisfactory description of the frequencies and polarization vectors of phonon modes.

2.3 Experimental optical studies of phonon modes

In recent years, the techniques of Raman scattering of light and IR absorption were used for detailed studies of isotopic effects in phonon spectra. In the first place, optical measurements were taken for the homeopolar crystals. The spectra for high-quality diamond single crystals were obtained and analyzed over the entire range of isotopic compositions from pure ^{12}C to pure ^{13}C [100–104] as well as for isotopically enriched germanium crystals and ultimately, isotopically 'contaminated' samples $^{70}Ge_{0.5}$ $^{76}Ge_{0.5}$ [105, 106]. Also studied were α-Sn [107] and silicon [108]. Then measurements were carried out for phonons in diatomic semiconductors. The group of M Cardona (Stuttgart) studied the compounds CuCl (using the isotopes ^{63}Cu, ^{65}Cu, ^{35}Cl, ^{37}Cl) [109], GaN (^{14}N, ^{15}N) [110], ZnSe (^{64}Zn, ^{68}Zn, ^{76}Se, ^{80}Se) [111], SiC (^{28}Si, ^{30}Si) [112], GaP (^{69}Ga, ^{71}Ga) [113, 114], and CuCl [109]. Let us discuss the main results obtained by optical methods.

2.3.1 Homeopolar crystals. *One-phonon processes.* The crystals of diamond, silicon and germanium belong to the symmetry group O_h^7. Their primitive cell contains two atoms. The crystal lattice may be regarded as involving two mutually penetrating face-centered cubic lattices shifted one with respect to the other in the direction of the diagonal of the cube. The lattices are displaced by one-fourth of the diagonal of the unit cube. The photon–phonon interaction in the case of one-phonon inelastic processes may only encompass phonons with the wave vector $\mathbf{q} \approx 0$.

For the crystals under consideration, the symmetry group of point Γ (the center of the Brillouin zone) coincides with the group of directions O_h. In the case of Raman scattering, the phonons are scattered from the fluctuations of the electron polarizability induced by atomic vibrations in the crystal lattice. The optically active mode in first-order Raman spectra is the mode with the F_{2g} symmetry (Fig. 8). This mode is three-fold degenerate, and is often denoted as LTO(Γ). In the scattering processes involving this mode the components $P_{xz}^{(1)}$, $P_{yz}^{(1)}$ of a polarization tensor are nonzero. The first-order Raman spectrum consists of separate delta-shaped lines. As far as IR scattering is concerned, the optical modes $\mathbf{q} \approx 0$ corresponding to the displacement of two similar atoms do not give rise to an electric dipole moment parallel to the photon electric field vector, and so there is no light absorption.

By definition, in the virtual crystal approximation, the LTO-mode frequency at the point Γ is $\omega_{\mathrm{LTO}} \propto M_{\mathrm{c}}^{-1/2}$. In the single-isotope samples, the mode lifetime τ depends on the anharmonic phonon interaction. In this case the dependence of phonon anharmonic damping $\Gamma_{\mathrm{a}} \sim \tau_{\mathrm{a}}^{-1}$ is found from the following considerations. At $T = 0$, the quantity Γ_{a} is

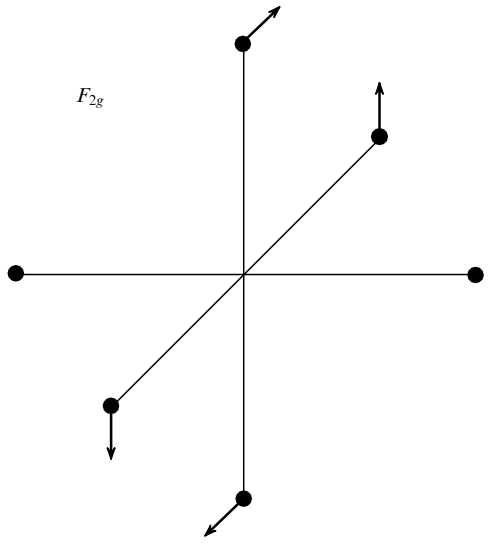

Figure 8. Basis vectors of the F_{2g} irreducible representation at the point Γ — the center of the Brillouin zone for an LTO-phonon.

proportional to the parameter squared of the anharmonic interaction ($\sim M_c^{-3/2}$) and to the density of two-phonon states ($\sim M_c^{1/2}$), so that $\Gamma_a \sim M_c^{-1}$. In the region $T \geqslant T_D/3$, owing to the temperature dependence of the occupation numbers ($\sim T/T_D$), we have $\Gamma_a \sim TM_c^{-1/2}$. A similar dependence on the mass is exhibited by the phonon frequency shift owing to anharmonism [115] (see also recent paper [116]). Thus, one obtains

$$\omega_{LTO}(M,T) = \begin{cases} aM^{-1/2} - bM^{-1}, & \text{if} \quad T \ll T_D, \\ aM^{-1/2} - b_1 TM^{-1/2}, & \text{if} \quad T > \dfrac{T_D}{3}. \end{cases}$$

In crystals made up of different isotopes, one needs to take into account the processes of elastic phonon scattering by isotope impurities. They give rise to an impurity-related frequency shift Δ_{iso} and to additional damping Γ_{iso}. Since the theory contains the small parameter ξ^2, it is possible to provide a satisfactory quantitative description of the experiments even in the Born approximation of perturbation theory. In this situation, Δ_{iso} and Γ_{iso} are described by relations (2.32) and (2.33).

Calculations based on the coherent potential method and the supercell method give similar results. The inclusion of elastic impurity scattering in samples with isotopic disorder should lead to a departure from the linearity of shift and damping as functions of the average mass M_c.

Let us discuss at greater length the experimental results for C, Si, Ge, and α-Sn crystals. As found later [106], in the early experiments with germanium [105, 107] the quality of surface polishing and the presence of surface oxide film prevented one from getting sufficiently reliable data. The results of subsequent experiments [106] turned out to be in very good agreement with the theory (the coherent potential approximation, supercell method), including such a delicate issue as the description of second-order effects with respect to the isotope mass difference. It was found that compared with the isotopically pure ^{70}Ge crystal, the additional frequency shift Δ_{iso} of an optical phonon at the point Γ was 0.34 ± 0.04 cm^{-1} for germanium samples with a natural isotopic composition, and 1.06 ± 0.04 cm^{-1} for the artificially prepared maximally disordered isotopic composition, containing approximately 50% of ^{70}Ge and 50% of ^{76}Ge. Since for germanium at the point Γ the density of phonon states is $\rho \approx 0$, we thus have $\Gamma_{iso} \approx 0$. A similar pattern of the phonon shift and damping was found with Si [108] and α-Sn [107].

Experimental findings for the Raman frequency and damping as functions of the mean mass for different isotope compositions in Ge [106] and α-Sn [107] are shown in Figs 9 and 10. The phonon frequencies vary as $aM^{-1/2}$. Slight deviations for the isotopically pure samples are associated with anharmonic effects. Deviations in samples with isotopic disorder are much more pronounced. From these diagrams we also see that the isotopic disorder leads to additional phonon damping. It is easy to prove that the standard anharmonic shift according to the experiment is approximately one order of magnitude greater than Γ_{iso}.

Diamond is an exception. For this material, the ultimate optical phonon frequencies are shifted with respect to the center of the Brillouin zone, so that the density of states at the point Γ is nonzero. It was found that upon transition from the composition $^{12}C_{0.35}{}^{13}C_{0.65}$ to the natural composition, the values of shift and damping renormalizations for the Raman mode are $\Delta_{iso} \approx 2$ cm^{-1} and $\Gamma_{iso} \approx 6$ cm^{-1}, respectively [100,

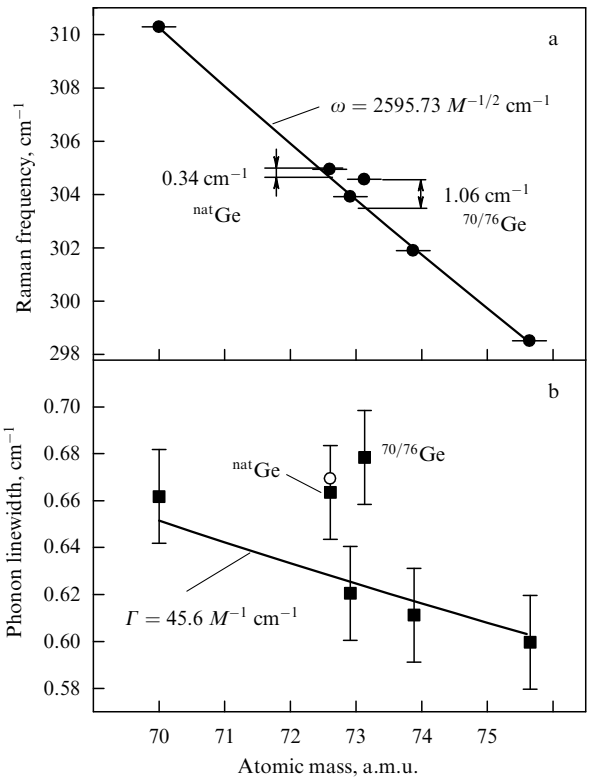

Figure 9. Frequency (a) and linewidth (b) of an optical phonon as functions of the mean atomic mass for isotopically enriched and disordered germanium samples at 10 K. The theoretical value of the phonon linewidth for isotopically pure germanium with an atomic mass $M = 72.6$, calculated from first principles [118], is marked with a circle [107].

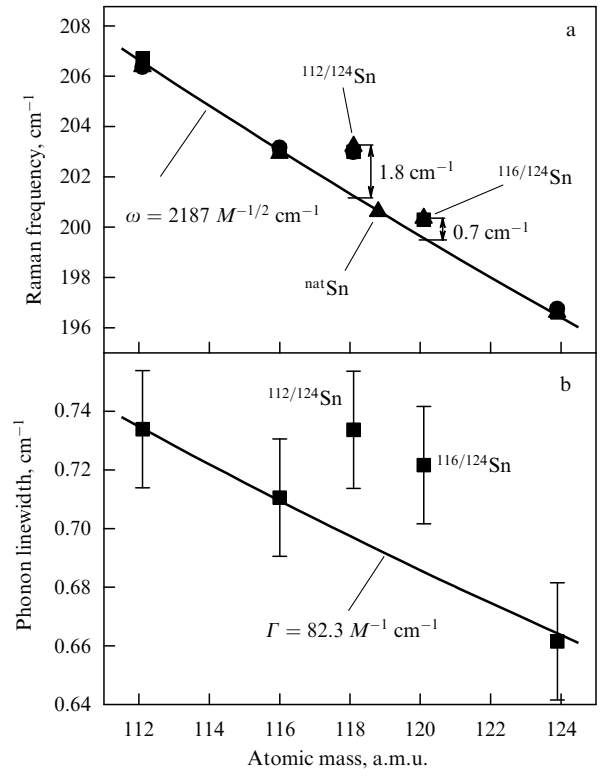

Figure 10. Raman frequency (a) and linewidth (b) of an optical phonon as functions of the mean atomic mass for five α-Sn thin films of different isotopic compositions at ~ 10 K. Solid line on the bottom diagram depicts the anticipated anharmonic behavior of isotopically pure samples [108].

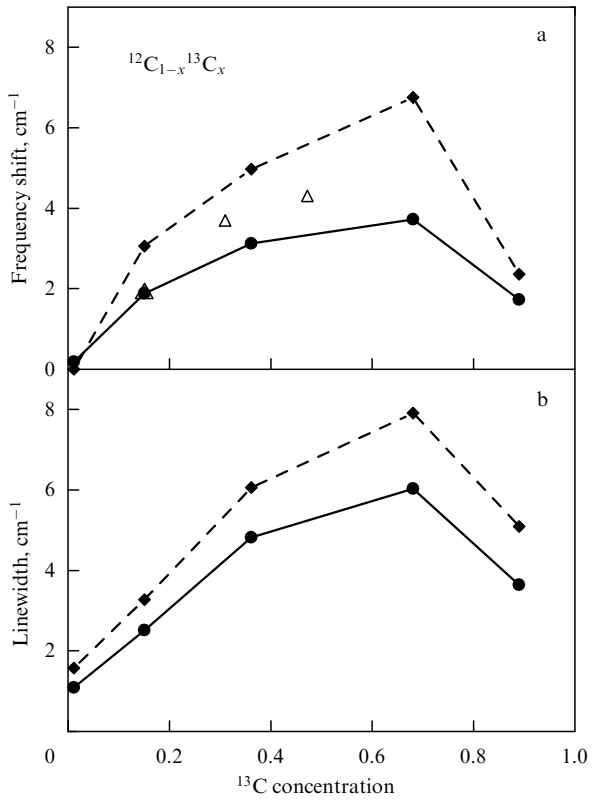

Figure 11. Raman shift (a) and linewidth (b) in diamond as functions of the concentration of the isotope ^{13}C. The experimental points were taken from Refs [100] (◆) and [123] (Δ). The solid lines passing through the circles represent the theoretical results obtained by Vast and Baroni [48].

101, 119–121]. Figure 11 shows the values of experimental frequencies and linewidths for several isotopic compositions $^{12}C_{1-x}{}^{13}C_x$, as well as the corresponding theoretical magnitudes obtained by the supercell method [48, 122].

We ought also to mention the works [104, 124] concerned with studying Raman scattering of light in diamond and germanium with different isotopic compositions at high pressure (up to 14 and 10 GPa, respectively). The results indicate that the interatomic forces in diamond and germanium act differently. It was found that in the case of diamond the frequency ratio $\omega(^{12}C)/\omega(^{13}C)$ starts to deviate from the classical value given by $[M(^{12}C)/M(^{13}C)]^{-1/2}$ with increasing pressure, decreasing by several percent from its value at $P = 0$. The authors suggested that this deviation is associated with the manifestation of Coulomb type forces. In the case of germanium, the dependence $\omega(P)$ for isotopically pure samples is described by the common curve $\omega M_c^{1/2}$. At the same time, for natural germanium the relevant curve does not coincide with the $\omega M_c^{1/2}$ line because of the isotopic disorder.

Two-phonon processes. Absorption and scattering of photons may also occur via two-phonon processes, when their total momentum is $\mathbf{q}_1 + \mathbf{q}_2 \approx 0$. In a two-phonon process, either two phonons are produced with equal and oppositely directed wave vectors, or one phonon is created and the other annihilated. This mechanism is associated with the terms of type $P^{(2)}$, standing for the crystal polarizability, which are proportional to the second degree of mode coordinates. In the case of IR radiation scattering, the two-phonon processes also bring about the formation of *continuous* second-order spectra. Then the first phonon distorts the charge distribution of adjacent atoms and induces the electric charge, while the second phonon displaces the charge, thus giving rise to the electric dipole moment.

Knowing the behavior patterns of the phonon mode frequencies and their concrete values, one can find the density of the two-phonon combination states:

$$\rho_2(\omega) = \sum_{j1\,j2} \int \frac{\mathrm{d}\sigma_{j1\,j2}}{\nabla\left[\omega(\mathbf{q}j1) + \omega(\mathbf{q}j2)\right]}\,, \tag{2.40}$$

where the relation $\omega(\mathbf{q}j1) + \omega(\mathbf{q}j2) = \text{const}$ defines a surface element $\mathrm{d}\sigma_{j1\,j2}$ in the $\mathbf{q}$-space. It is important that the distribution $\rho_2(\omega)$ exhibits analytical singularities (peaks and points of inflections). These critical points are defined by the following condition:

$$\nabla\left[\omega(\mathbf{q}j1) + \omega(\mathbf{q}j2)\right] = 0\,.$$

The critical points under consideration fall into three groups:

(1) $\nabla\left[\omega(\mathbf{q}j1)\right] = \nabla\left[\omega(\mathbf{q}j2)\right] = 0$. These are the well studied van-Hove singularities for separate phonon branches.

(2) $\nabla\left[2\omega(\mathbf{q}j1)\right] = 0$. This condition is satisfied by the high-symmetry points of Γ, X, W, and L type.

(3) $\nabla\left[\omega(\mathbf{q}j1)\right] = -\nabla\left[\omega(\mathbf{q}j2)\right] \neq 0$. This condition holds for diamond type crystals in the direction Σ.

In the analysis of spectra one has to take into account the selection rules that reduce the number of the overtones realized (both modes have the same symmetry type) and combination tones (the modes have different symmetry types). For example, in the case of Raman scattering the polarizability is characterized by the symmetrical tensor of the second order, which is transformed on the basis of the representation $[F_{1u}]^{(2)}$. Then we have the resolution of the form

$$[F_{1u}]^{(2)} = A_{1g} + E_g + F_{2g}$$

which determines the active modes. In the case of IR absorption, the electric dipole moment vector has the symmetry F_{1u}. We find the corresponding active modes by resolving representations $[\Gamma_n]^2$ (the case of overtones) and $\Gamma_n \otimes \Gamma_n$ (combination tones) into irreducible states. Observe that for IR radiation scattering all overtones are forbidden.

The second-order Raman and IR spectra for high-quality diamond samples with natural isotopic composition and those samples rich in ^{13}C (1.3% ^{12}C and 98.7% ^{13}C) were experimentally studied in detail by Vogelgesang et al. [125] (see also Ref. [103]). The corresponding diagrams are shown in Figs 12 and 13. It is interesting to note that the spectra for ^{13}C and $^{\text{nat}}$C practically coincide to the smallest detail, if we scale the frequencies in terms of the average mass as $M_c^{-1/2}$, in accordance with the virtual crystal approximation. In this situation, the effects quadratic with respect to the isotope mass difference turn out to be rather small compared to the linear effect. The theory of representations was used in work [125] for identifying the realizable types of active modes for different critical points; the calculated frequencies of both acoustic and optical modes were in very good agreement with experiment (see numbered points in Figs 12, 13 and Table 2). The appropriate values are close to those obtained by neutron spectroscopy. Generally speaking, the accuracy of optical data is better than that of neutron spectroscopy by an order of

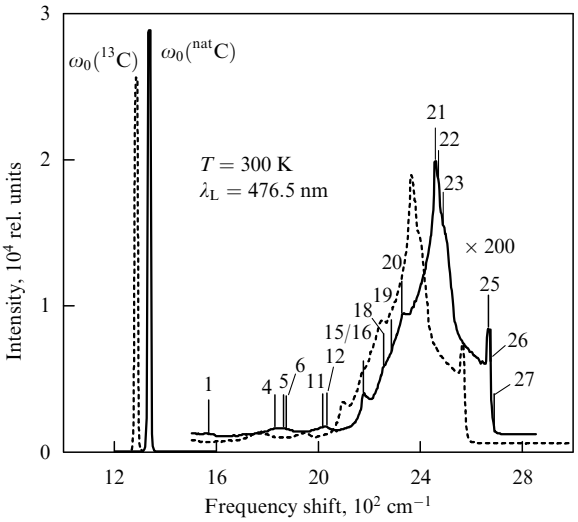

Figure 12. Raman spectrum of natural diamond (98.9% ^{12}C) (solid line) and diamond enriched in ^{13}C up to 98.7% (dashed line). The dominant first-order line F_{2g} which is active in the Raman spectrum, and the much more weaker many-phonon quasi-continuous peculiarities are shown. Two-phonon peculiarities are marked with numbers in accordance with Table 2 [103, 125].

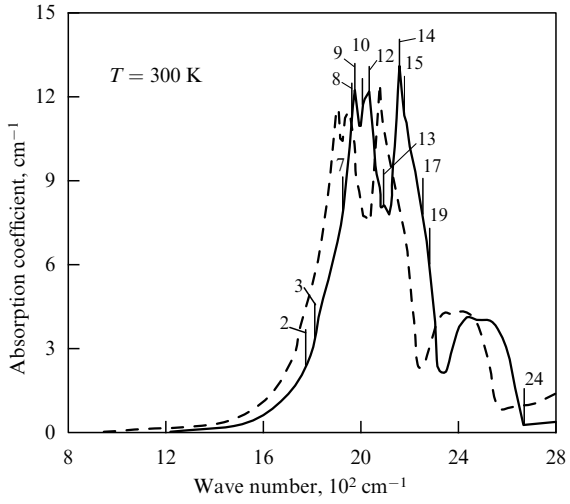

Figure 13. Many-phonon singularities in natural diamond (solid line) and ^{13}C diamond (dashed line) in the IR absorption spectrum (the first-order line is absent). Two-phonon singularities are marked with numbers in accordance with Table 2 [103, 125]. Mode $F_{2g}(q \approx 0)$ is not active in the IR spectrum.

magnitude. It should be recorded that knowledge of the acoustic mode frequencies has allowed the values of elastic moduli and their dependence on the isotopic composition to be obtained (for details see Ref. [103]).

Table 2. Phonon combinations and overtones for the Brillouin-zone critical points in diamond.

No.	**q**, $2\pi/a$	Assignment	Activity				ω, cm^{-1}	
			Raman spectrum			IR spectrum		
			$\Gamma^{(1+)}$	$\Gamma^{(12+)}$	$\Gamma^{(25+)}$	$\Gamma^{(15-)}$	Experiment	Theory [125]
1	(1, 0, 0)	$[X^{(3)}(\mathrm{TA})]^{(2)}$	1	1	1	0	1569	1572
2	(1/2, 1/2, 1/2)	$L^{(3-)}(\mathrm{TO}) \otimes L^{(3+)}(\mathrm{TA})$	0	0	0	2	1780	1780
3	(1/2, 1/2, 1/2)	$L^{(3+)}(\mathrm{TA}) \otimes L^{(2-)}(\mathrm{LO})$	0	0	0	1	1817	1817
4	(1, 1/2, 0)	$[W^2(\mathrm{TA})]^{(2)}$	1	1	1	0	1829	1830
5	$\sim 0.78\times$ (1, 1, 0)	$\Sigma^{(2)}(\mathrm{O}) \otimes \Sigma^{(4)}(\mathrm{A})$	0	0	1	1	1863	1863
6	(1, 0, 0)	$X^{(3)}(\mathrm{TA}) \otimes X^{(4)}(\mathrm{TO})$	0	1	0	1	1874	1874
7	(1, 1/2, 0)	$W^{(1)}(\mathrm{TO}) \otimes W^{(2)}(\mathrm{TA})$	0	1	2	2	1927	1927
8	(1, 0, 0)	$X^{(1)}(\mathrm{L}) \otimes X^{(3)}(\mathrm{TA})$	0	0	1	1	1959	1956
9	$\sim 0.75\times$ (1, 1, 0)	$\Sigma^{(1)}(\mathrm{A}) \otimes \Sigma^{(3)}(\mathrm{A})$	0	0	1	1	1977	1977
10	$\sim 0.84\times$ (1,1,0)	$\Sigma^{(1)}(\mathrm{O}) \otimes \Sigma^{(4)}(\mathrm{A})$	0	1	0	1	2007	2007
11	(1/2, 1/2, 1/2)	$[L^{(1+)}(\mathrm{LA})]^{(2)}$	1	0	1	0	2017	2018
12	$\sim 0.70\times$ (1, 1, 0)	$\Sigma^{(3)}(\mathrm{O}) \otimes \Sigma^{(3)}(\mathrm{A})$	1	1	1	1	2034	2034
13	$\sim 0.70\times$ (1, 1, 0)	$\Sigma^{(2)}(\mathrm{O}) \otimes \Sigma^{(3)}(\mathrm{A})$	0	1	0	1	2095	2096
14	$\sim 0.75\times$ (1, 1, 0)	$\Sigma^{(2)}(\mathrm{O}) \otimes \Sigma^{(3)}(\mathrm{O})$	0	1	0	1	2158	2157
15	(1, 1/2, 0)	$W^{(1)}(\mathrm{TO}) \otimes W^{(2)}(\mathrm{L})$	0	1	2	2	2176	2176
16	(1, 0, 0)	$[X^{(4)}(\mathrm{TO})]^{(2)}$	1	1	1	0	2176	2176
17	(1/2, 1/2, 1/2)	$L^{(2-)}(\mathrm{LO}) \otimes L^{(1+)}(\mathrm{LA})$	0	0	0	1	2254	2254
18	(1, 0, 0)	$X^{(1)}(\mathrm{L}) \otimes X^{(4)}(\mathrm{TO})$	0	0	1	1	2256	2258
19	$\sim 0.73\times$ (1, 1, 0)	$\Sigma^{(1)}(\mathrm{O}) \otimes \Sigma^{(3)}(\mathrm{O})$	0	0	1	1	2286	2287
20	(1, 1/2, 0)	$[W^{(2)}(\mathrm{L})]^{(2)}$	1	1	1	0	2328	2328
21	$\sim 0.50\times$ (1, 1, 0)	$[\Sigma^{(1)}(\mathrm{O})]^{(2)}$	1	1	1	0	2460	2460
22	$\sim 0.70\times$ (1, 1, 0)	$[\Sigma^{(1)}(\mathrm{O})]^{(2)}$	1	1	1	0	2472	2472
23	(1/2, 1/2, 1/2)	$[L^{(2-)}(\mathrm{LO})]^{(2)}$	1	0	1	0	2490	2490
24	(0, 0, 0)	—	HF limit of IR-active combinations				2665	2664.8
25	—	—	Overtones associated with the topmost optical branch				2667	—
26	—	—					2676	—
27	—	—					2690	—

2.3.2 Diatomic semiconductors. *First-order Raman spectra.* Raman spectra of the first order for diatomic GaN crystal with wurtzite structure were taken by Zhang et al. [110].

Measurements were performed with specimens of the following isotopic composition: $Ga^{15}N$, $^{nat}Ga\,^{14}N_{0.5}\,^{15}N_{0.5}$, and $Ga^{14}N$. The vibrational modes LO and TO were studied. The Brillouin zone for GaN is a hexagonal prism. Representations of the group of a wave vector at the point Γ coincide with the representations of the point group C_{6v}. Optically active are the modes with A_1, E_1, and $2E_2$ symmetries (Fig. 14). In the case of polar A_1, E_1 modes, both the atoms (gallium and nitrogen) move in the same direction. Such a motion can be described in terms of the effective reduced mass $\mu^{-1} = M_1^{-1} + M_2^{-1}$. For the non-polar E_2 mode these atoms move in antiparallel directions. The corresponding two modes constitute a mixture of Ga and N vibrations.

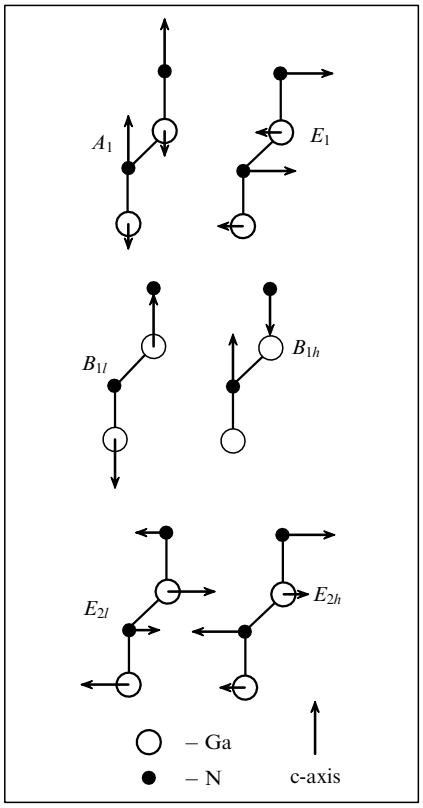

Figure 14. Eigenvectors of irreducible representations realized at the point Γ for optical phonons in GaN. The representations $B_{1l}(E_{2l})$ and $B_{1h}(E_{2h})$ relate to low-frequency and high-frequency modes B_1 (E_2) [111].

In the harmonic approximation, the two modes with E_2 symmetry can be phenomenologically described as follows.

Consider the motion of two coupled oscillators with masses M_1 and M_2. Then we have

$$M_1\ddot{X}_1(t) = -K_1X_1(t) - K_{12}X_2(t)\,, \tag{2.41a}$$

$$M_2\ddot{X}_2(t) = -K_2X_2(t) - K_{21}X_1(t)\,. \tag{2.41b}$$

Here K is the matrix of force parameters. In the standard approach, when $X_j(t) = X_j\exp(i\omega t)$, in place of equations (2.41) we have in the operator form:

$$K\mathbf{X} = \lambda\mathbf{X}, \quad \lambda = \omega^2\,. \tag{2.42}$$

Then the eigenfrequencies are defined as

$$\omega_{1,2}^2 = \frac{1}{2}\,(\Omega_1^2 + \Omega_2^2) \pm \sqrt{(\Omega_1^2 - \Omega_2^2)^2 + \frac{4K_{12}^2}{M_1M_2}}\,, \tag{2.43}$$

where

$$\Omega_1^2 = \frac{K_1}{M_1}\,, \quad \Omega_2^2 = \frac{K_2}{M_2}\,. \tag{2.44}$$

Our treatment also involves orthonormalized eigenvectors, for which we go over from the matrix equation (2.42) to an equation in the form

$$M^{1/2}KM^{-1/2} \times M^{1/2}\mathbf{X} = \lambda M^{1/2}\mathbf{X}\,. \tag{2.45}$$

Notice that in addition to equations (2.41)–(2.45) we also have relations (2.8) which connect the isotopic frequency shift with the modulus squared of the corresponding polarization vector.

Experimental results were used by Zhang et al. [110] for finding the elements of the matrix of force parameters and then the eigenvectors on the basis of the above approach. It was found that the gallium atom moves almost entirely in the low-frequency mode, and the nitrogen atom in the high-frequency mode. In work [110] results are also reported of microscopic calculations based on the theory of the density functional. As found, the theory gives a reasonably accurate description of the observed values of both frequencies and polarization vectors.

Raman spectra for several polytypes (3*C*, 6*H*, 15*R*) of silicon carbide SiC were obtained in Ref. [112]. The specimens were natural superlattices with two different isotopic compositions with respect to silicon (the carbon isotopic composition was invariably the same, i.e. natural). One specimen contained silicon with natural isotopic composition, whereas the other was highly enriched in ^{30}Si (5.0% ^{28}Si, 1.3% ^{29}Si, 93.7% ^{30}Si). The spectra for 6*H* and 15*R* polytypes allow reconstruction of the dispersion curves for longitudinal and transverse optical and acoustic modes in the $\Gamma - L$ direction. Knowledge of the experimental frequencies for the two isotopic compositions allowed Widulle et al. to find the polarization vectors in the framework of the same model as used for GaN, with due account for relation (2.42). The following conditions were additionally imposed on the phases of acoustic modes:

$$e_C = e(C)\exp\left[i\Phi(C)\right], \quad e_{Si} = \sqrt{1 - e^2(C)} = e(Si)\,. \tag{2.46}$$

The polarization vectors for optical modes are obtained by making the replacements $\Phi \to \Phi + \pi$, $e(C) \to e(Si)$ ($\mathbf{e} = M^{1/2}\mathbf{X}$). The authors of Ref. [112] compared their results with the calculations for frequencies and polarization vectors carried out with the bond-charge model. The concordance between theory and experiment in this case should be regarded as a two-way street.

Recently, Rohmfeld et al. [126] studied the Raman spectra for two SiC polytypes (6*H* and 15*R*) with different isotopic compositions with respect to carbon; it was experimentally demonstrated that the isotopic broadening of phonon modes Γ_{iso} is proportional to the density of phonon states $\rho(\omega)$ [see

formula (2.30)]. This linear relation was observed over a range of values covering one order of magnitude. The absolute value $|\mathbf{e}(\mathrm{C})|$ of the polarization vector for the carbon sublattice, found from the coefficient of proportionality, fits in well with both the experimental results of Ref. [112] and the theoretical findings of Karch et al. [95] derived from first principles.

Anomalous Raman spectra for TO-phonons. Fermi resonance. In works [113, 114] the anomalous shape of the first-order Raman spectrum observed for the transverse optical phonon in the case of GaP crystals was studied. The shape of the spectral lines for specimens ^{71}GaP, $^{69}Ga_{0.4}{}^{71}Ga_{0.6}P$, $^{69}Ga_{0.6}{}^{71}Ga_{0.4}P$, and ^{69}GaP was investigated.

A specimen with natural isotopic composition displayed an asymmetrical broadened peak. Such broadening is associated with processes related to cubic anharmonism. Owing to the anharmonic interaction, the optical TO(Γ)-phonon with a frequency ω_0 decomposes into longitudinal and transverse acoustic phonons, so that the damping $\Gamma(\omega)$ equals the modulus squared of the anharmonic constant $|V_3|^2$ times the density $\rho_2(\omega)$ of the corresponding two-phonon states:

$$\Gamma(\omega) = |V_3|^2 \rho_2(\omega)\,. \tag{2.47}$$

Then the line shift is given by the formula

$$\widetilde{\Delta}(\omega) = \frac{2}{\pi}|V_3|^2 \int_0^{\omega_m} \mathrm{d}\omega'\, \frac{\omega' \rho_2(\omega')}{\omega^2 - \omega'^2}\,. \tag{2.48}$$

Concrete calculations reveal that the density of two-phonon states displays a weak-dispersion curve with a van-Hove singularity ω_k at the upper edge of the acoustic spectrum. The characteristic frequency ω_{TO} of the optical phonon is close to ω_k, which gives rise to a kink in the low-frequency part of the Raman spectrum (to the left of the maximum). As the isotopic composition is varied, the frequencies change as follows: $\omega_{\mathrm{TO}} \sim \mu_{\mathrm{GaP}}^{-1/2}$ and $\omega_k \sim M_{\mathrm{Ga}}^{-1/2}$ (by definition, $\mu_{\mathrm{GaP}}^{-1} = M_{\mathrm{Ga}}^{-1} + M_{\mathrm{P}}^{-1}$). Such a behavior of the frequencies ω_k is explained by the fact that in the acoustic modes in the first approximation it is the atoms of gallium that move. In the case of the TO mode, both Ga and P atoms are active. This is the reason why the relative disposition of frequencies ω_{TO} and ω_k on the frequency scale is changed, which leads to the change in the asymmetry of the peak (Figs 15, 16).

It should be noted that the spectra for the anharmonic constant were analyzed under the assumption [116]

$$|V_3|^2 \propto \mu_{\mathrm{GaP}}^{-1/2} M_{\mathrm{Ga}}^{-1/2} M_{\mathrm{P}}^{-1/2}\,. \tag{2.49}$$

Göbel et al. [109] analyzed a compound with the structure of zinc blende. Specimens were prepared from isotopes ^{63}Cu, ^{65}Cu, ^{35}Cl, and ^{37}Cl; the measurements were carried out at 2 K. Observe that the material in question is then close to a phase transition. The parameter of anharmonism is relatively large here. The Raman spectrum displayed peaks associated with the longitudinal and transverse optical phonons. The transverse phonon spectrum turned out to be anomalous. It consists of two peaks, broad and narrow (Fig. 17). The authors studied the dependence of these peaks on the isotopic composition of the specimens.

It is pertinent to note that the CuCl phonon spectrum is fairly well simulated in the microscopic approach. One can also calculate the anharmonic linewidth associated with the decomposition into two acoustic phonons [see formulas (2.47), (2.48)]. It is important that the frequency of a longitudinal phonon is considerably higher than the acoustic edge of the two-phonon spectrum. The frequency of the transverse mode lies lower, but near the spectrum edge. *By contrast to GaN, here we have a high density ρ_2 of states near*

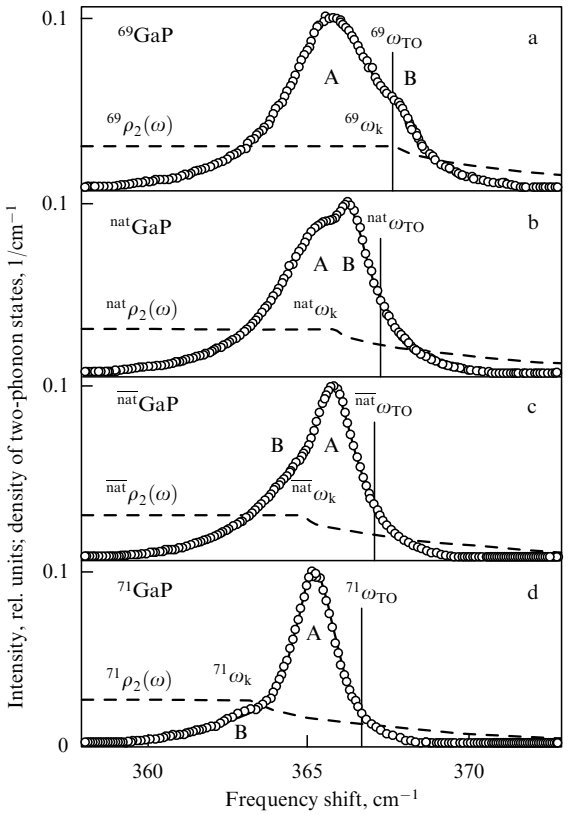

Figure 15. Raman spectra of TO-phonons in ^{69}GaP (a), $^{\mathrm{nat}}$GaP [$^{69}Ga_{0.6}{}^{71}Ga_{0.4}P$] (b), $^{\overline{\mathrm{nat}}}$GaP [$^{69}Ga_{0.4}{}^{71}Ga_{0.6}P$] (c), and ^{71}GaP (d) at $T = 6$ K. The solid lines represent fitted experimental data; the dashed lines depict the density of two-phonon states, and the vertical lines show the peaks of harmonic TO-phonons before renormalization [114].

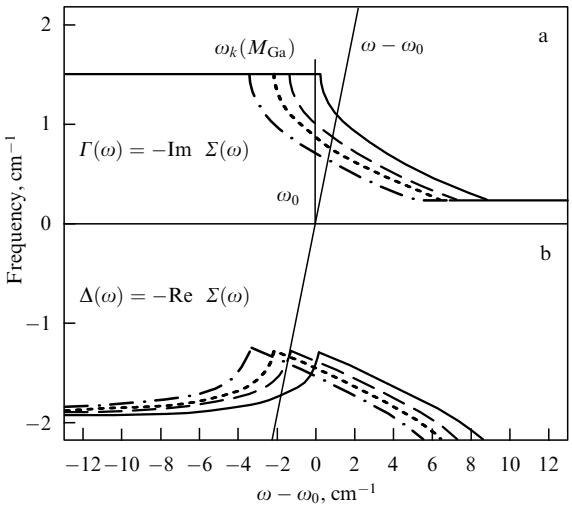

Figure 16. Anharmonic damping (a) and shift (b) of a TO-phonon in GaP: solid lines — ^{69}GaP, dashed lines — $^{\mathrm{nat}}$GaP, dotted lines — $^{\overline{\mathrm{nat}}}$GaP, dot-and-dash lines — ^{71}GaP. The harmonic phonon is marked with a vertical line, and its frequency serves as the reference point ($\omega_0 = 367.5 \pm 0.5$ cm^{-1}) [114].

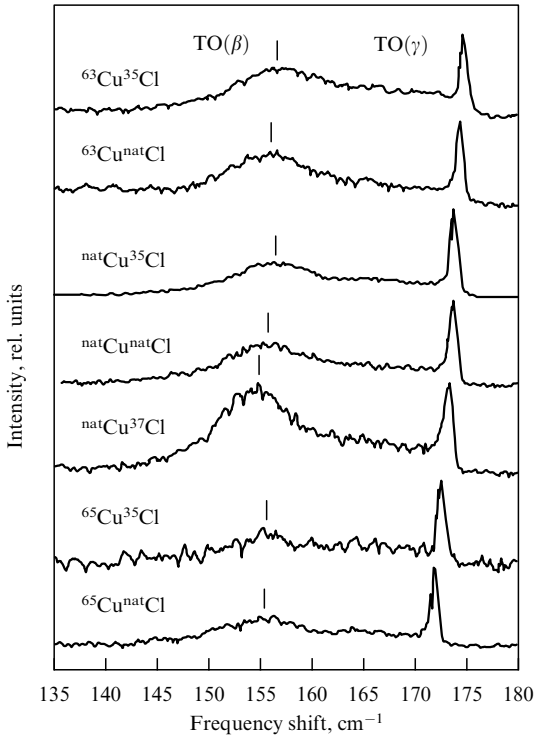

Figure 17. Raman spectra for the anomalous TO-peak for CuCl with different isotopic compositions. The reduced mass μ increases from the top to bottom of the diagram. The line TO(γ) only shifts when the content of copper isotopes is varied. The broad line TO(β) shifts when the reduced mass is varied [109].

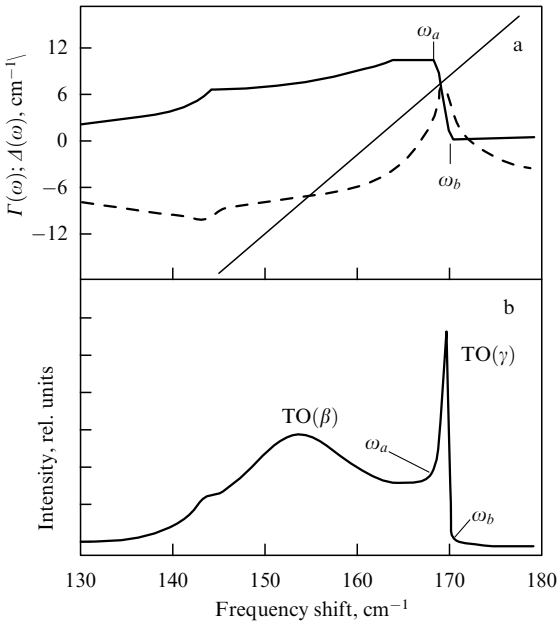

Figure 18. Fermi resonance for the TO-phonon anomaly in CuCl. The solid line on the diagram (a) shows the imaginary part of the phonon anharmonic eigenenergy $\Gamma(\omega)$, and the dashed line shows the frequency shift $\Delta\omega$. The straight line corresponds to the quantity ω–ω_{TO}. Diagram (b) shows the theoretical spectrum for ^{nat}Cu ^{nat}Cl [109].

the edge. The parameter of anharmonicity in CuCl is also higher but has the same order of magnitude. According to the theory, the frequencies of the boundary acoustic modes are $\sim M_{Cu}^{-1/2}$, and the optical frequencies are $\sim \mu_{CuCl}^{-1/2}$.

The authors of paper [109] gave a quantitative description of the observed anomalous transverse phonon spectrum. Its peculiarities can be treated in terms of Fermi resonance (Fig. 18). Namely, the transverse phonon interacts with the two-phonon state (biphonon). A certain 'repulsion' of energy levels occurs. The upper level is narrow, and its position mainly depends on the mass of the copper atom, which fits in with the experiment. The lower broad level is associated with an optical phonon which has a large probability of anharmonic decay and depends on the reduced mass.

2.4 Study of phonon spectra in germanium by inelastic neutron scattering

Optical methods give relatively limited information about the lattice vibration spectrum. The availability of precision first-order Raman spectra only permits the study of optical phonons near the center of the Brillouin zone. As regards the second-order Raman or photoluminescence spectra, they carry indirect information, again with a restricted ensemble of phonon modes at the symmetric points of the Brillouin zone. At the same time, the inelastic neutron scattering method, in principle, allows us to get complete information about the vibrational spectrum of a crystal (which implies that both the frequencies and the polarization vectors of the modes are measured in experiment). However, the as yet considerable instrumental width and the anharmonic effects still hamper the use of neutron spectroscopy in the studies of isotopic effects. Nevertheless, in the case of strong isotopic disorder, the modern techniques yield valuable quantitative information.

In this connection we should note that the effects of isotopic disorder on frequencies and damping of phonons in germanium were studied by Göbel et al. [73]. Measurements were taken at room temperature. The neutron spectra were obtained for two germanium specimens: isotopically pure ^{70}Ge (99.99%) and ultimately, isotopically disordered $^{70}Ge_{0.5}{}^{76}Ge_{0.5}$. The behavior of optical phonon modes for the symmetrical directions Δ_5 and Σ_3 was studied in detail (Fig. 19). In particular, it was confirmed that the frequencies varied as $\sim M_c^{-1/2}$. Most importantly, however, the corresponding values for frequency shifts Δ_{iso} and linewidths Γ_{iso}, proportional to ξ^2, were measured and analyzed. Notice that the phonon frequencies ω were of the order of 300 cm^{-1}, and the instrumental width was about 13 cm^{-1}. The experimental values of Δ_{iso} and Γ_{iso}, defined as the difference between the magnitudes for $^{70}Ge_{0.5}{}^{76}Ge_{0.5}$ and ^{70}Ge, were of the order of 1–2 cm^{-1}. The frequencies for the isotopic alloy were found using the relevant data for the isotopically pure crystal ^{70}Ge. In this case, according to theoretical estimates for acoustic modes, the values of the parameters under consideration are smaller by an order of magnitude. The corresponding values of ω, Δ_{iso}, and Γ_{iso} are compiled in Table 3.

The analysis [73] was carried out using the coherent potential and supercell methods, which yielded similar results. Figure 20 shows experimental and theoretical values for Δ_{iso} and Γ_{iso}. By and large, the investigations have uncovered a good quantitative agreement between the theory and experiment for Γ_{iso}. At the same time, there is a certain systematic discrepancy for the frequency shift. The following assumption was made in Ref. [73]. Germanium, which has only four neighbors at the first coordination sphere, may exhibit short-range-order effects. Namely, the light (or heavy)

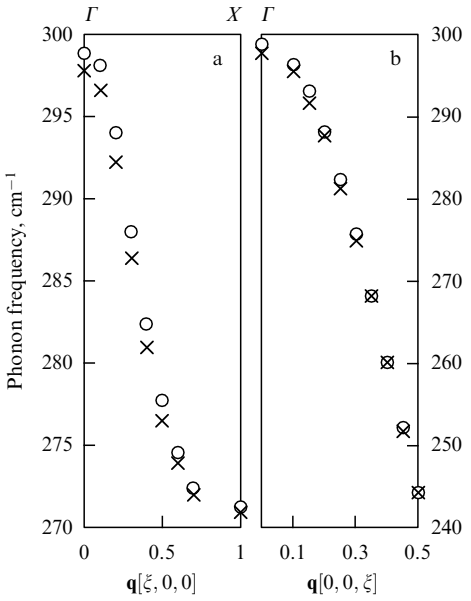

Figure 19. Phonon frequencies measured by inelastic neutron scattering at room temperature for ^{70}Ge (×) and $^{70/76}$Ge (○). The results for ^{70}Ge (×) were lowered by the factor 1.0227 to account for the trivial mass dependence: a — Δ_5(O), b — Σ_3(O) [73].

Table 3. Values of phonon mode frequencies ω, isotopic frequency renormalizations $\Delta_{\rm iso}$, and phonon widths $\Gamma_{\rm iso}$ for the crystal $^{70}Ge_{0.5}$ $^{76}Ge_{0.5}$ [73].

$\mathbf{q} = (q_x; q_y; q_z)$	ω, cm^{-1}	$\Delta(\Sigma_3(\mathrm{O}))$, cm^{-1}	$\Gamma(\Sigma_3(\mathrm{O}))$, cm^{-1}
(0.50;0.50;0)	244.1	0.18	0
(0.40;0.40;0)	260.2	0.18	0
(0.45;0.35;0)	268.2	0.01	1.41
(0.30;0.30;0)	275	0.77	2.34
(0.25;0.25;0)	281.3	1.07	2.14
(1.15;0.15;0)	291.6	1.51	1.44
(0.10;0.10;0)	295.5	0.96	0
$\mathbf{q} = (q_x; q_y; q_z)$	ω, cm^{-1}	$\Delta(\Delta_5(\mathrm{O}))$, cm^{-1}	$\Gamma(\Delta_5(\mathrm{O}))$, cm^{-1}
(1.0;0;0)	270.9	0.32	1.73
(0.7;0;0)	272.0	0.31	1.73
(0.6;0;0)	273.9	0.66	2.05
(0.5;0;0)	276,.	1.23	2.22
(0.4;0;0)	280.9	1.41	1.36
(0.3;0;0)	286.4	1.56	1.19
(0.2;0;0)	292.2	1.77	0.91
(0.1;0;0)	296.6	1.47	0

atoms are surrounded preferably by light (or heavy) atoms. The interaction is mainly short-ranged in character, which is the reason why the actual frequencies of vibrational modes in the isotopic alloy may differ from theoretical values obtained under the assumption of a random atomic distribution over the lattice sites.

3. Static displacements of lattice atoms near isotopic impurities

Atomic vibrations give a certain contribution to the bond energy and are known to affect the static configuration of the lattice atoms. When the lattice sites are occupied with different isotopes, the atoms will be displaced from equilibrium positions characteristic of an ideal crystal (chemically

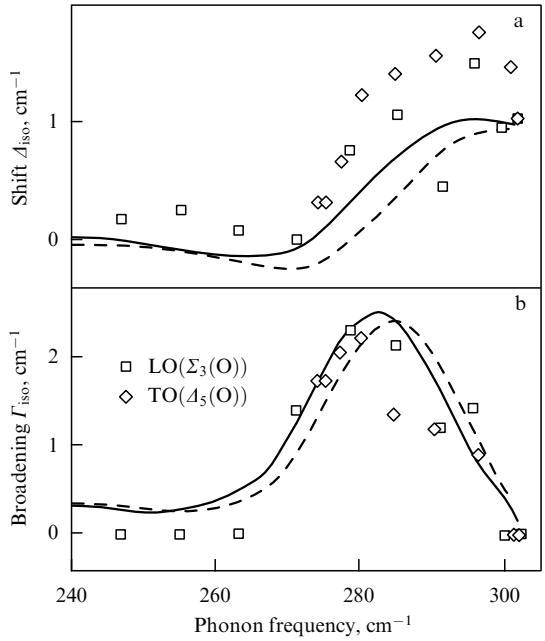

Figure 20. Phonon shift (a) and broadening (b) in germanium owing to isotopic disorder. The results obtained with the supercell method are represented by solid lines, and those obtained by the coherent potential method are represented by dashed lines. Calculations were done for the case of an isotopically disordered alloy with the disorder parameter $\xi^2 = 1.52 \times 10^{-3}$, similar to that of the actual specimen. The experimental errors in Δ and Γ were lower than 0.4 cm^{-1} [73].

pure and built of isotopes of the same kind). As a result, the fields of static displacements $\{\zeta_{\mathbf{n}}\}$ appear near the 'impurity' isotopes. The resulting dynamic disorder is described by the correlation function

$$K^{\alpha\beta}_{\mathbf{n}_1\mathbf{n}_2}(t=0) = \langle u^{\alpha}_{\mathbf{n}_1} u^{\beta}_{\mathbf{n}_2} \rangle \tag{3.1}$$

formed in terms of the operators of dynamic atomic displacements. Observe that in the range of temperatures, where the classical statistics holds, the correlator $K^{\alpha\beta}_{\mathbf{n}_1\mathbf{n}_2}(t=0)$ does not depend on the mass, and the fields of displacements disappear.

In this section we present theoretical results for statical displacements, obtained within the microscopic approach. We also find an asymptotic representation for $\{\zeta_{\mathbf{n}}\}$ in the limit when $|\mathbf{R}^{(0)}_{\mathbf{n}}|$ is much greater than the interatomic distance a. Also discussed are the results of NMR studies of the isotopic composition effects on the shape of spectral lines.

For the first time, the problem of static displacements of crystal lattice atoms in isotopically disordered solutions was formulated in the studies of kinetic properties of quantum crystals — the effects of ^{3}He impurities on thermal conductivity of a solid ^{4}He [127–129]. Most recently, the problem of static atomic displacements in isotopically disordered crystals has become the subject of investigation as applied to metals [130] and semiconductors [131, 132].

3.1 Dynamic disordering and static displacements near impurities

Let us consider a crystal lattice with isolated isotopic impurities. For the sake of simplicity we assume that

$$M_{\mathbf{n}} = M_0 + \Delta M \delta_{\mathbf{n},0}, \quad \Delta M = M_1 - M_0\,. \tag{3.2}$$

Here, M_0 is the mass of the regular matrix atom, and M_1 is the mass of an impurity isotope. The origin of the coordinates coincides with the equilibrium position of an impurity isotope.

The total energy E depends on the atomic coordinates $\mathbf{R_n}$. In a crystal with impurities, the atoms become displaced from their equilibrium positions $\mathbf{R}_\mathbf{n}^{(0)}$ in an ideal lattice, so that

$$\mathbf{R_n} = \mathbf{R}_\mathbf{n}^{(0)} + \boldsymbol{\zeta}_\mathbf{n} + \mathbf{u_n}\,, \tag{3.3}$$

where $\boldsymbol{\zeta}_\mathbf{n}$ is the vector of static displacements, and $\mathbf{u_n}$ is the vector of dynamic displacements.

Taking into consideration that the atomic displacements are small compared with the interatomic distances, we expand the structure-dependent part of the energy in a power series of $\mathbf{u}_n$ and $\boldsymbol{\zeta}_\mathbf{n}$ with respect to $\mathbf{R}_\mathbf{n}^{(0)}$. We would like to find the relaxation energy E_r associated with the static displacements of atoms near impurities, retaining the terms of the first and second order in $\zeta_\mathbf{n}$. In symbolic notation for the energy E_r we have

$$E_\mathrm{r} = F\zeta + \frac{1}{2}\,\Phi_2\,\zeta^2\,. \tag{3.4}$$

The effective force F in expression (3.4), acting on regular matrix atoms from the side of an impurity isotope and displacing them, can be represented as

$$F_\mathbf{n}^\alpha = \frac{1}{2}\sum_{\mathbf{n}_1\mathbf{n}_2} \Phi^{\alpha\beta\gamma}_{3,\mathbf{n}\mathbf{n}_1\mathbf{n}_2}\Delta K^{\beta\gamma}_{\mathbf{n}_1\mathbf{n}_2}\,. \tag{3.5}$$

The characteristic of dynamic disordering, ΔK, is defined as the difference between K-correlators for the lattice with an impurity isotope and regular lattice:

$$\Delta K^{\alpha\beta}_{\mathbf{n}_1\mathbf{n}_2} = K^{\alpha\beta}_{\mathbf{n}_1\mathbf{n}_2}(\Delta M \neq 0) - K^{\alpha\beta}_{\mathbf{n}_1\mathbf{n}_2}(\Delta M = 0)\,. \tag{3.6}$$

In equations (3.4)–(3.6), the force parameters of the second and third order, Φ_2 and Φ_3, and the K-correlator are defined with respect to the equilibrium atomic positions in an ideal lattice.

Assuming that the resultant force acting on the atom is zero, $\partial E_\mathrm{r}/\partial\zeta_\mathbf{n} = 0$, we find the set of equations in ζ:

$$F + \Phi_2\zeta = 0\,. \tag{3.7}$$

In the coordinate representation we find from this the following relations

$$\zeta_\mathbf{n}^\alpha = -\bar{D}^{\alpha\beta}_{\mathbf{n}\mathbf{n}'}F^\beta_{\mathbf{n}'}\,, \quad \bar{D} = (\Phi_2)^{-1}\,. \tag{3.8}$$

The relaxation energy E_r is then equal to $F\zeta/2$.

Let us express explicitly the correlator K determining the effective force F. First, we take into account the standard relation between the correlator $\langle u_\mathbf{n}(t)u_{\mathbf{n}'}(0)\rangle$ and one-particle Green function D. We have

$$\int_{-\infty}^{\infty} \mathrm{d}t\exp(-\mathrm{i}\omega t)K^{\alpha\beta}_{\mathbf{n}_1\mathbf{n}_2}(t) = \frac{2\mathrm{Im}\,D^{\alpha\beta}_{\mathbf{n}_1\mathbf{n}_2}(\omega - \mathrm{i}\delta)}{1-\exp(-\omega/T)}\,. \tag{3.9}$$

Taking into account that the Green function D satisfies an approximate relation of the form [see Eqn. (2.22)]

$$D^{\alpha\beta}_{\mathbf{n}\mathbf{n}'}(\omega) \approx D^{\alpha\beta}_{0,\mathbf{n}\mathbf{n}'}(\omega) + \omega^2\sum_{\mathbf{n}_1} D^{\alpha\gamma}_{0,\mathbf{n}\mathbf{n}_1}(\omega)(M_0 - M_{\mathbf{n}_1})D^{\gamma\beta}_{0,\mathbf{n}_1\mathbf{n}'}(\omega)\,, \tag{3.10}$$

we might use expressions (3.9) and (3.10) and find for the case of an isolated impurity:

$$\Delta K^{\alpha\beta}_{\mathbf{n}_1\mathbf{n}_2}(t=0) \approx \approx -\frac{2\Delta M}{\pi}\int_{-\infty}^{\infty}\mathrm{d}\omega\,\frac{\omega^2}{1-\exp(-\omega/T)}\,\mathrm{Im}\big[D^{\alpha\gamma}_{0,\mathbf{n}_1\mathbf{0}}(\omega)D^{\gamma\beta}_{0,\mathbf{0}\mathbf{n}_2}(\omega)\big], \tag{3.11}$$

where the 'zero' Green function D_0 of an ideal crystal lattice is presented in the form

$$D^{\alpha\beta}_{0,\mathbf{n}\mathbf{n}'}(\omega + \mathrm{i}\delta) = \frac{1}{M_0 N}\sum_{\mathbf{q}j} e_\alpha(l)e_\beta(l)\,\frac{\exp\big[\mathrm{i}\mathbf{q}(\mathbf{R}_\mathbf{n}^{(0)} - \mathbf{R}_{\mathbf{n}'}^{(0)})\big]}{\omega^2 - \omega^2(l) + \mathrm{i}\delta\,\mathrm{sign}\,\omega}\,. \tag{3.12}$$

The knowledge of the factor ΔK allows us to find the field of static atomic displacements, based on relation (3.5). For the spatial Fourier component $\zeta^\alpha_\mathbf{n}$ we get the following expression

$$\zeta^\alpha(\mathbf{q}) = \sum_j \bar{D}^{\alpha,\beta}_{\mathbf{q}j}F^\beta(\mathbf{q})\,, \tag{3.13a}$$

where

$$\bar{D}^{\alpha,\beta}_{\mathbf{q}j} = \frac{e_\alpha(l)e_\beta(l)}{M_0\omega^2(l)}\,, \tag{3.13b}$$

$$F^\alpha(\mathbf{q}) = -\frac{1}{2}\,\frac{\Delta M}{M_0}\sum_{\mathbf{q}_1\mathbf{q}_2 j_1 j_2}\Phi^{\alpha\beta\gamma}_{3,qq_1q_2}Z^{\beta\gamma}_{\mathbf{q}_1\mathbf{q}_2}\,, \tag{3.13c}$$

$$Z^{\alpha\beta}_{\mathbf{q}_1\mathbf{q}_2} = \sum_{j_1 j_2} e_\alpha(l_1)e_{\gamma_1}(l_1)e_{\gamma_1}(l_2)e_\beta(l_2) \times \frac{\omega(l_1)\big[2n\big(\omega(l_1)\big)+1\big] - \omega(l_2)\big[2n\big(\omega(l_2)\big)+1\big]}{M_0\big[\omega^2(l_1) - \omega^2(l_2)\big]}\,. \tag{3.13d}$$

From the last formula it follows that at absolute zero of temperature we have

$$Z^{\alpha\beta}_{\mathbf{q}_1\mathbf{q}_2}(T=0) = \sum_{j_1 j_2}\frac{e_\alpha(l_1)\,e_{\gamma_1}(l_1)\,e_{\gamma_1}(l_2)\,e_\beta(l_2)}{M_0\big[\omega(l_1)+\omega(l_2)\big]}\,. \tag{3.14}$$

In the limit of high temperatures we have $Z = 0$, and therefore the field of static displacements near the isotopic impurity disappears.

Let us make some estimates for the linear chain model with the interaction between nearest neighbors. In this model, the spatial Fourier components of the force parameters of the second, f_2, and third, g_3, orders — that is, $\Phi_{2,q}$ and Φ_{3,qq_1q_2} — are represented as (see, for example, monograph [133])

$$\Phi_{2,q} = M_0\omega_q^2\,, \quad M_0\omega_q^2 = 4f_2\sin^2\frac{qa}{2}\,, \tag{3.15}$$

$$\Phi_{3,qq_1q_2} = -\frac{\mathrm{i}g_3}{(f_2/M_0)^{3/2}}\;\tilde{\omega}_q\tilde{\omega}_{q_1}\tilde{\omega}_{q_2}\Delta(q+q_1+q_2)\,, \tag{3.16}$$

$$\tilde{\omega}_q = 2\left(\frac{f_2}{M_0}\right)^{1/2}\sin\frac{qa}{2}\,.$$

Here a is the lattice constant. As regards the relationship between parameters f_2 and g_3, it is known that for the central force model and the integral Grüneisen parameter $\gamma_\mathrm{G} \approx 2$ we have $-g_3a/f_2 \approx 10$.

Based on the relations (3.13), (3.14) and making use of equations (3.15), (3.16), we arrive at the following estimate for static displacements of atoms located on the first coordination sphere relative to the isotopic impurity:

$$\zeta \approx -0.3\epsilon\,\frac{g_3 a^2}{f_2} \sim -\epsilon a\,, \quad \epsilon = \frac{\Delta M}{M_0}\,\frac{\langle u^2\rangle}{a^2}\,, \tag{3.17}$$

where $\langle u^2\rangle$ is the mean square of the dynamic atomic displacements. Notice that ϵ is a characteristic parameter of the theory. From the last relations it follows that because of the difference in zero vibrations *the lattice contracts near the heavy isotope and expands near the light isotope*. In common solids we have $\langle u^2\rangle/a^2 \sim 10^{-3}$ and $|\Delta M|/M_0 \leqslant 0.1$, so that $|\epsilon| \leqslant 10^{-4}$. Thus we see that the static atomic displacements near impurities are very small compared with the distance between the atoms.

It would be interesting to make similar estimates for quantum crystals. Let some lattice sites in an ^{4}He matrix be occupied with ^{3}He isotopes. Using the values for the Debye temperature $T_D = 26$ K and the lattice constant $a = 3.57$ Å, reported in Ref. [127], we then get $\langle u^2\rangle/a^2 \approx 3\times 10^{-2}$. Since $|\Delta M|/M_0 = 0.25$, the static displacements are noticeable. On the first coordination sphere $\zeta = 0.025$. These displacements are of the same order as those for systems with nonisotopic impurities.

3.2 Asymptotic representation for the field of static displacements

Let us derive the expression for $\boldsymbol{\zeta}_{\mathbf{n}}$ in the asymptotic limit, when $|\mathbf{R}_{\mathbf{n}}^{(0)}|$ is much greater than the interatomic distance a. By definition, we have

$$\zeta_{\mathbf{n}}^{\alpha} = \frac{\Omega_0}{(2\pi)^3}\int \mathrm{d}\mathbf{q}\,\exp\bigl(\mathrm{i}\mathbf{q}\mathbf{R}_{\mathbf{n}}^{(0)}\bigr)\zeta^{\alpha}(\mathbf{q})\,, \tag{3.18}$$

where Ω_0 is the unit cell volume. We shall assume that the integrand in formula (3.18) is analytical. Then at $|\mathbf{R}_{\mathbf{n}}^{(0)}| \gg a$, owing to the fast oscillation of the term $\sin \mathbf{q}\mathbf{R}_{\mathbf{n}}^{(0)}$, the main contribution to the integral comes from the range of small $\mathbf{q}$ coming from the directions almost perpendicular to the vector $\mathbf{R}_{\mathbf{n}}^{(0)}$.

We represent the quantity $\zeta^{\alpha}(\mathbf{q}\to 0)$ defined by Eqn (3.13a) in the form

$$\zeta^{\alpha}(\mathbf{q}\to 0) = \sum_j -\mathrm{i}\bar{D}^{\alpha\beta}_{\mathbf{q}\to 0,j}\,q^{\beta}\lim_{\mathbf{q}\to 0}\mathrm{i}\widetilde{F}(q),$$

$$\lim_{\mathbf{q}\to 0}\widetilde{F}(q) = \frac{F^{\beta}(\mathbf{q}\to 0)}{q^{\beta}}\,. \tag{3.19}$$

Let us substitute relation (3.19) into formula (3.18) and perform the integration in Eqn (3.18) over the interval $(0,\infty)$. Having regard to the estimate $\zeta(\mathbf{q}\to 0)\sim q^{\alpha}/q^2$, we get

$$\zeta_{\mathbf{n}}^{\alpha} \sim d_{\mathrm{im}}\,\frac{A^{\alpha}(\mathbf{n}_{\circ})}{\mathbf{R}_{\mathbf{n}}^2}\,, \quad \mathbf{n}_{\circ} = \frac{\mathbf{R}_{\mathbf{n}}}{|\mathbf{R}_{\mathbf{n}}^{(0)}|}\,. \tag{3.20a}$$

Here the following notation was used:

$$d_{\mathrm{im}} = \lim_{\mathbf{q}\to 0}\mathrm{i}\widetilde{F}(q)\,, \tag{3.20b}$$

$$A^{\alpha}(\mathbf{n}_{\circ}) = \frac{1}{8\pi^2}\int_0^{2\pi}\mathrm{d}\varphi\left[\frac{\partial}{\partial\theta}\sum_j \frac{e_j^{\alpha}(\theta,\varphi)\bigl(\mathbf{e}_j(\theta,\varphi)\mathbf{q}_{\circ}\bigr)}{M_{\mathrm{c}}v_j(\theta,\varphi)}\right]_{\theta=\pi/2}. \tag{3.20c}$$

It should be pointed out that the standard factor $A^{\alpha}(\mathbf{n}_{\circ})$ is expressed in terms of the polarization vectors and velocities of sound $v_j(\theta,\varphi)$ in a regular lattice; in addition $\mathbf{q}_{\circ} = \mathbf{q}/|\mathbf{q}|$ and the polar angle θ is measured with respect to $\mathbf{n}_{\circ}$. The factor A describes the angular dependence of $\boldsymbol{\zeta}_{\mathbf{n}}$; it bears no relation to the properties of the impurity isotope. In the case of crystals with cubic symmetry, the analytical formulas for $A^{\alpha}(\mathbf{n}_{\circ})$ have been obtained for $\boldsymbol{\zeta}_{\mathbf{n}}$ aligned with the directions [100], [110], and [111] (see, respectively, Refs [134 – 136]).

Now let us find the quantity d_{im}. Taking into account that

$$\left(\frac{\partial}{\partial q_{\alpha}}\,\Phi^{\alpha_1\alpha_2\alpha_3}_{3,\,\mathbf{q}\mathbf{q}_1\mathbf{q}_2}\right)_{\mathbf{q}\to 0}$$

$$= -\mathrm{i}\sum_{\mathbf{n},\mathbf{n}_1,\mathbf{n}_2}\exp(-\mathrm{i}\mathbf{q}_1\mathbf{R}_{\mathbf{n}_1}^{(0)})\exp(-\mathrm{i}\mathbf{q}_2\mathbf{R}_{\mathbf{n}_2}^{(0)})R^{(0)}_{\mathbf{n},\alpha}\,\Phi^{\alpha_1\alpha_2\alpha_3}_{3,\,\mathbf{n}\mathbf{n}_1\mathbf{n}_2}\,, \tag{3.21a}$$

we may use the recurrent relation for the force parameters of different orders in the form

$$\sum_{\mathbf{n}_1} R^{(0)}_{\mathbf{n}_1,\alpha}\Phi^{\alpha_1\ldots\alpha_{p+1}}_{p+1,\,\mathbf{n}_1\ldots\mathbf{n}_{p+1}} = \Omega_0\,\frac{\partial}{\partial\Omega_0}\,\Phi^{\alpha_2\ldots\alpha_{p+1}}_{p,\,\mathbf{n}_2\ldots\mathbf{n}_{p+1}}\delta_{\alpha\alpha_1} \tag{3.21b}$$

(see, for example, Refs [133, 137]). Considering expression (3.14) for $Z_{\mathbf{q}_1\mathbf{q}_2}$, we get as an upshot

$$d_{\mathrm{im}} \approx -\frac{\Delta M}{2M_0}\sum_l\sum_{\mathbf{m}}\Omega_0\,\frac{\partial}{\partial\Omega_0}\,\Phi^{\alpha\beta}_{2,\mathbf{0m}}\exp\bigl(\mathrm{i}\mathbf{q}\mathbf{R}_{\mathbf{m}}^{(0)}\bigr)\frac{e_{\alpha}(l)e_{\beta}(l)}{2\omega(l)}\,. \tag{3.22}$$

As the volume is varied, the change of the eigenvalue (frequency squared) in the first approximation is equal to the corresponding diagonal element of the perturbation energy taken over the unperturbed states. Therefore, one obtains

$$\frac{\partial\omega^2(l)}{\partial\Omega} = e_{\alpha}(l)\,\frac{\partial\Phi^{\alpha\beta}_{2,\,\mathbf{q}}}{\partial\Omega}\,e_{\beta}(l)\,. \tag{3.23}$$

Using this relation, in place of formula (3.22) we get

$$d_{\mathrm{im}} \approx -\frac{\Delta M}{M_0}\,\frac{\partial E_{\mathrm{vib}}}{\partial\Omega}\,, \quad E_{\mathrm{vib}} = \frac{1}{2}\sum_l \hbar\omega(l)\,,$$

where E_{vib} is the zero-vibration energy.

The derivative $\partial E_{\mathrm{vib}}/\partial\Omega$ can be expressed in terms of the change $\Delta\widetilde{\Omega}$ in the unit cell volume, which arises as a result of variation of precisely the isotopic composition (see paper [138]). Then we have

$$\frac{\Delta M}{M_0}\,\frac{\partial E_{\mathrm{vib}}}{\partial\Omega} \approx -B_0\,\frac{\Delta\widetilde{\Omega}}{\Omega_0}\,,$$

where B_0 is the bulk compression modulus, and

$$d_{\mathrm{im}} \approx B_0\,\frac{\Delta\widetilde{\Omega}}{\Omega_0}\,.$$

In calculating the quantities that are integral with respect to the field of static displacements, on the qualitative level it is often sufficient to rely on the elastic isotropic continuum approximation. In such a case it is possible to arrive at an explicit expression for $\boldsymbol{\zeta}_{\mathbf{n}}$. With this purpose we define the

quantity

$$C^{\alpha} = \frac{1}{N}\sum_{l} \bar{D}_{l}^{\alpha\beta} q^{\beta} \exp\left(\mathrm{i}\mathbf{q}\mathbf{R}_{\mathbf{n}}^{(0)}\right). \tag{3.24}$$

In the case of isotropic continuum, the polarization vectors of longitudinal (l) and transverse (t) modes satisfy the following relations

$$\mathbf{e}^{(l)}(q) = \frac{(\mathbf{q}\mathbf{n})\mathbf{q}}{q^2}, \quad \mathbf{e}^{(l)} \perp \mathbf{e}^{(t)}, \tag{3.25}$$

where $\mathbf{n}$ is the unit vector. In view of these relations we can demonstrate that after summation over the polarization branches j only the contribution from the longitudinal modes is retained in formula (3.24). Their frequencies are given by

$$\omega^{(l)}(q) = \sqrt{\frac{\lambda+\mu}{\rho q}}, \tag{3.26}$$

where λ and μ are the Lamé coefficients, ρ is the density, and

$$\frac{M_0(\lambda+2\mu)}{\rho} = \Omega_0 c_{11}. \tag{3.27}$$

Here c_{11} is the modulus of elasticity. As a result we get the following relations

$$\begin{aligned} C^{\alpha} &= \frac{-\mathrm{i}}{M_0 N}\sum_{\mathbf{q}} \frac{q^{\alpha}\exp\left(\mathrm{i}\mathbf{q}\mathbf{R}_{\mathbf{n}}^{(0)}\right)}{\omega^{(l)2}(q)} \\ &= \frac{1}{\Omega_0 c_{11}} \frac{\partial}{\partial R_{\mathbf{n},\alpha}^{(0)}} \frac{\Omega_0}{2\pi^3}\int \mathrm{d}\mathbf{q}\, \frac{\exp\left(\mathrm{i}\mathbf{q}\mathbf{R}_{\mathbf{n}}^{(0)}\right)}{q^2} \\ &= -\frac{1}{4\pi}\frac{1}{c_{11}}\frac{R_{\mathbf{n},\alpha}^{(0)}}{R_{\mathbf{n}}^3}. \end{aligned} \tag{3.28}$$

From these relations, we finally get (see Ref. [130])

$$\zeta_{\mathbf{n}} \approx \frac{b}{4\pi}\frac{\mathbf{R}_{\mathbf{n}}^{(0)}\Omega_0}{|\mathbf{R}_{\mathbf{n}}^{(0)}|^3}, \quad b = \frac{\Delta\widetilde{\Omega}}{\Omega_0}\frac{B_0}{\Omega_0 c_{11}}, \tag{3.29}$$

where b is the defect capacity.

In the case of an elastic isotropic continuum, the field of atomic displacements is purely radial. The static displacements in a crystal are anisotropic. The displacements become radial only along the symmetric directions and demonstrate more complex behavior along the nonsymmetric directions. On the coordination spheres nearest to the impurity, the values of $\zeta_{\mathbf{n}}$ calculated by formulas (3.13) and (3.18) differ by a factor of 2 or 3. The values calculated by the asymptotic formula are in excess of the true ones. Notice that the asymptotic limit for $\zeta_{\mathbf{n}}$ is actually realized only at $|\mathbf{R}_{\mathbf{n}}^{(0)}| \geqslant (4-5)a$, i.e. starting with the 6th–8th coordination spheres (see, for example, Ref. [139]). Nevertheless, relation (3.18) gives the correct sign and scale of the displacement. For illustration, Figs 21 and 22 show the fields of displacements ζ in the bcc ^{7}Li lattice that arise around the light isotopic impurity ^{6}Li. The static displacements were calculated on the basis of the pseudopotential theory. Straightforward definitions of the force parameters in the second and third order, using the local pseudopotentials, are given in Ref. [130].

In the case of metals, the electron multiports require, in general, special treatment. If the Fermi surface is spherical,

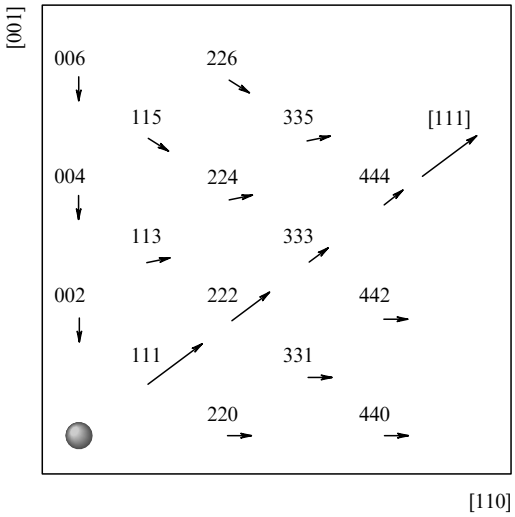

Figure 21. Static atomic displacements around the light isotopic impurity ^{6}Li in the bcc ^{7}Li lattice. Displacements are given in arbitrary units and projected onto the plane [110]. The location of impurity is indicated with circle.

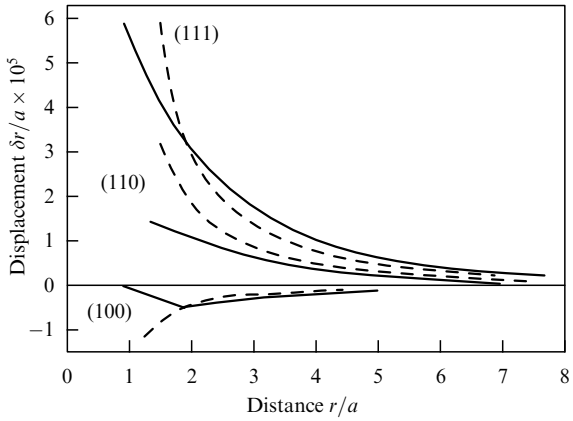

Figure 22. Radial static atomic displacements around the impurity ^{6}Li in ^{7}Li for three directions [111], [110], and [100]. Solid lines correspond to calculations done using the exact equations for the fields of displacements, and dashed lines correspond to calculations from the asymptotic formula.

the expression for ζ contains an oscillating term that decreases as R^3. If the Fermi surface is entirely cylindrical or flat, the Kohn singularity is reinforced, and the asymptotic expression for ζ changes [140].

Theoretical analysis of the fields of displacements around isotopic defects has been carried out in few works (see Refs [127–130]). In Ref. [127], in connection with the problem of thermal conductivity of solid ^{4}He containing ^{3}He impurities, it was suggested that the lattice gets distorted near the impurity isotopes. The atomic displacements are expressed in terms of such quantities as the zero-vibration energy in spherical potential well and the relaxation energy due to the inclusion of a finite radius. Glyde [128] considered ^{3}He with ^{4}He as an impurity, and the displacements $\delta R/R$ on the coordination spheres closest to the impurity were calculated in the framework of the self-consistent harmonic approximation. It was found that $\delta R/R \sim 0.01$, and the force interaction parameters are considerably renormalized because of static displacements. A more comprehensive theory based on the self-consistent harmonic Kohler approach was developed by

Jones [129]. This theory allows us to estimate the effects of displacements at large distances from the defect, and thus provides for a more accurate description of the long-wavelength-phonon scattering. The theory in Ref. [130] was formulated in terms of Green functions. The equation derived for $\zeta_{\mathbf{n}}$ involves the microscopic parameters. The explicit form of the atomic displacements is given in the asymptotic limit.

The chaotic distribution of interatomic distances, resulting from the superposition of the fields of static displacements near the isotopes, may be important for various phenomena. Some of these are discussed below. We shall analyze the situation when the chaotic distribution of electric fields in the crystal, caused by static displacements, may lead to the broadening of NMR lines, when the magnetic nucleus exhibits a quadrupole electrical moment. Static displacements of atoms and local variations of the crystal lattice elastic properties may considerably reduce thermal and electric conductivities of crystals. Such fields of displacements, for example, can essentially modify the residual electrical resistance ρ_r of chemically pure metals containing different isotopes, and their contribution to ρ_r is greater than the contribution caused by the difference in the dynamic amplitudes of elastic electron scattering.

3.3 NMR measurements of static displacements in germanium single crystals

Static displacements of crystal lattice atoms near isotopic impurities can be studied by the nuclear magnetic resonance method. The necessary condition for observing displacements is the presence of at least two kinds of isotopic impurities in the lattice. These are, firstly, the isotopes with nonzero nuclear magnetic and quadrupole moments. It is on the nuclei of such isotopes that nuclear magnetic resonance is registered. Secondly, it is the impurity isotopes with a zero nuclear moment. In such a situation, if near the probe nucleus there is an impurity isotope of a different kind, the arising local distortions of the crystal lattice will modify the electric field gradient on the probe nucleus. As a result, the energy levels of nuclei with a *nonzero* nuclear quadrupole moment in the neighborhood of the defect will exhibit a quadrupolar shift, which will lead to broadening of the NMR line. This effect is especially clear when in an ideal lattice (without impurities) the electric field gradient at the lattice site is zero. Such a situation is realized in crystals with the cubic symmetry of the nucleus charge environment.

Recently, Verkhovskii and his colleagues [131, 132] discovered the effects of isotopic disorder in NMR spectra of ^{73}Ge nuclei in isotopically modified germanium single crystals. Figure 23 shows NMR spectra taken with two germanium specimens with approximately the same concentrations of ^{73}Ge nuclei in a magnetic field of 12 T at room temperature. One specimen was highly enriched in ^{70}Ge (96.3% ^{70}Ge, 2.1% ^{72}Ge, 0.1% ^{73}Ge, 1.2% ^{74}Ge, and 0.3% ^{76}Ge) and in this experiment appeared as an almost regular crystal with a narrow NMR line. The other specimen had almost equal concentrations of ^{70}Ge and ^{76}Ge (43% ^{70}Ge, 2% ^{72}Ge, $\sim 0.1\%$ ^{73}Ge, 7% ^{74}Ge, and 48% ^{76}Ge) and was a crystal with the practically highest possible isotopic disorder parameter ξ^2. Its NMR line was much broader. The lattice cubic symmetry, the fairly high quadrupole moment of ^{73}Ge nuclei ($I = 9/2$, $eQ = -0.19$ barn), and their low concentration in the specimens that allowed the neglect of the direct dipole–dipole interaction between nuclear magnetic moments, all these features ensured a high sensitivity of the NMR experiment on the detection of small local static lattice distortions around the resonance nuclei. The fact that there are no other germanium isotopes with a nonzero nuclear magnetic moment also facilitated the experiment.

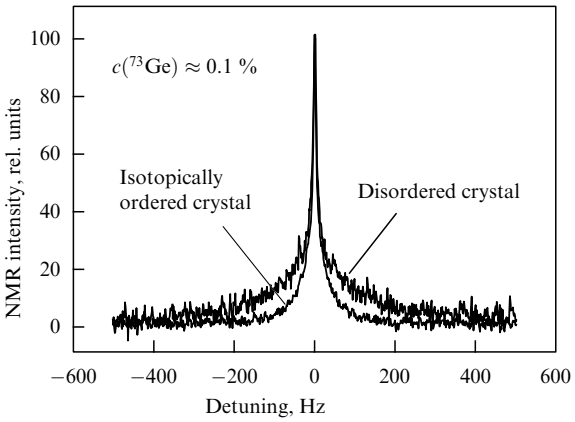

Figure 23. Shape of ^{73}Ge NMR line in two germanium single crystals with different isotopic compositions: isotopically ordered (96.3% ^{70}Ge) and isotopically disordered (43% ^{70}Ge + 48% ^{76}Ge) samples. The spectra were taken in 12-T magnetic field directed along the crystallographic axis [111] at $T = 300$ K [141].

Local deformations of the germanium crystal lattice around the impurity isotope ^{73}Ge and the quadrupole broadening of the NMR line, induced by the isotopic disorder, were simulated using the adiabatic bond-charge model for the case when the crystal matrix was built up from the isotopes ^{74}Ge [131]. The local deformations of the lattice were primarily analyzed. The atomic displacements are presented in Table 4. Let us comment on these results. Since the mass of the probe nucleus is different from that of the matrix nuclei, it creates local lattice distortions in its neighborhood: the light atom 'pushes apart' the surrounding matrix atoms. The radial displacements δr of atoms on the first coordination sphere around a single impurity isotope are about -1.5×10^{-5} Å at $T = 0$ K, and they decrease with increasing temperature to -0.36×10^{-5} Å at room temperature, which is comparable with the size of a nucleus itself. The displacements of atoms on the second coordination sphere are smaller by about an order of magnitude. These lattice distortions, however, do not induce an electric field on the probe nucleus. The local electric fields on the probe nucleus are created by a 'pair' of impurity isotopes, and the field will be the strongest when the separation between these isotopes is of the same order of magnitude as the interatomic distance in the lattice. Since in

Table 4. Atomic displacements caused by isotopic impurity centers in germanium crystals. The theoretical results are given in units of 10^{-5} Å per amu mass change [131].

Type of impurity center	Parameter	Temperature, K			
		0	80	300	450
Single impurity atom	δr	−1.47	−1.06	−0.36	−0.19
Pair of nearest neighbors	δr^f	−2.04	−1.37	−0.50	−0.22
	δr_1^f	−1.59	−1.18	−0.43	−0.19
Pair of second nearest neighbors	δr^s	−1.80	−1.36	−0.50	−0.22

this experiment the concentration of ^{73}Ge was $\sim 0.1\%$, only the impurity isotope dimers were considered (Fig. 24). Calculations confirmed that because of the correlation between atomic displacements of impurity atoms in dimers, their mutual displacements δr^f along the pair axis are increased by about 40% (Fig. 24a). The radial displacements δr_1^f of the six nearest matrix atoms in such a system also turn out to be important. In the pair of impurities next to nearest neighbors (Fig. 24b), the displacements of the impurity atoms themselves can be neglected, but a considerable displacement (δr^s) is exhibited by the matrix atom being the common nearest neighbor to both the 'foreign' atoms. Theoretical results on the fields of atomic and charge displacements around isotopic impurities were used for calculating the random crystal electric fields, the interactions of the nuclear quadrupole moments with these fields, and the relevant effects in NMR spectra. The model spectra are in qualitative agreement with experiment.

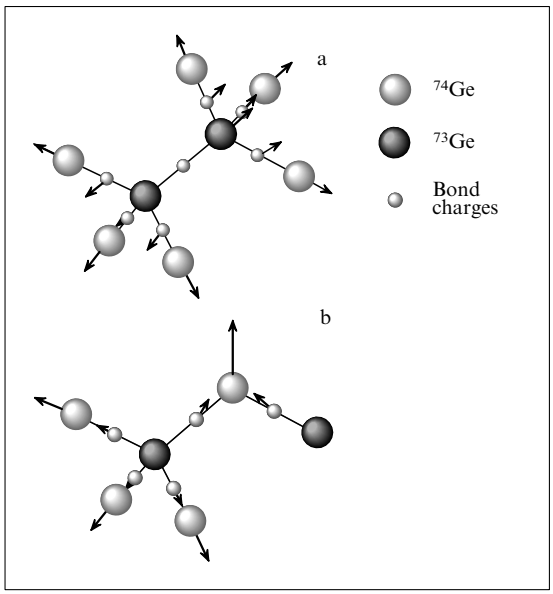

Figure 24. ^{73}Ge impurity pairs of the first (a) and second (b) nearest neighbors in a ^{74}Ge crystal lattice [131].

The experimental sensitivity to local deformations of crystal lattice ($\sim 10^{-5}$ Å) was almost an order of magnitude better than that of the traditional X-ray and neutron diffraction methods. Accordingly, in some cases the NMR technique may be considered as a powerful tool for controlling the crystal lattice perfection.

To end this section, we note that the problem of inhomogeneous broadening of resonance lines in NMR, EPR and other spectra, caused among other things by static atomic displacements, was discussed in detail theoretically in the review [142] (see also the review [143] and paper [144]). We should also point out theoretical studies [145, 146] concerned with the effects of crystal lattice deformation (under the action of generalized external forces) and the related symmetry lowering on the spectra of impurity atoms.

4. Conclusions

The most straightforward indications of the effects of isotopes on the properties of solids are the isotopic effects observed in the phonon spectra. The effects of the first and second orders are studied currently with respect to the isotope mass difference, using optical and neutron spectroscopy methods for a broad variety of monatomic and polyatomic semiconductors. These studies validated and improved the contemporary models of dynamic interatomic interaction in covalent crystals. In addition, the studies of materials with complicated crystal lattices 'have honed' the coherent potential and supercell methods used for describing the phonon modes in nonideal systems.

In crystals, because of fluctuations of zero vibrations and anharmonism, static fields of atomic displacements $\{\zeta_{\mathbf{n}}\}$ arise around the impurity isotopes. The analysis of atomic configurations arising near the isotopic impurities with due account for their mutual influence has just started for specific materials. Static displacements in germanium crystals were recently studied for the first time using the nuclear magnetic resonance method as applied to ^{73}Ge. This experiment demonstrated a very high sensitivity to small (on the order of 10^{-5} Å) local lattice deformations around the resonant nucleus. Such a sensitivity is an order of magnitude better than that achieved with the traditional X-ray and neutron diffraction techniques.

We thank L A Maksimov for attentively reading the manuscript and for valuable comments and advice, and A Yu Yakubovskiĭ for useful discussions and for making available to us the experimental NMR data prior to their publication. We are grateful to V Yu Baranov for his attention and support. A P Zhernov expresses his gratitude to Yu M Kagan and N A Chernoplekov for their support. His work was partly financed by RFFI (grant 01-02-16508), and by the RAS State Research Grant. The work of A V Inyushkin was partly sponsored by RFFI (grant 01-02-17469) and by CRDF (grant #RP2-2274).

5. Appendix. Bond-charge model

The bond-charge model firstly formulated by Weber [147, 148] explicitly takes into account the directional nature of atomic bonds in ion-covalent crystals. Such an asymmetry of interactions is due to the presence of peaks in the electron density distributions over the regions of covalent bonds (they have been experimentally studied, for example, using the X-ray diffraction technique). In this model, in addition to the positive charges on the atomic ion cores, inertialess negative point charges of the covalent bonds are introduced [bond charges (BCs)], and the Coulomb interaction between all charges of both types is taken into consideration. The principle of adiabaticity is also postulated: for any particular configuration of cores, the BCs arrange themselves in such a way as to minimize the total energy. In doing so, the adiabatically displaced BCs are used for describing the many-particle nature of the interaction between the ions.

Observe that in the case of heteropolar crystals, the equilibrium position of the BC shifts towards the more electronegative atom. The characteristics of BCs for various cores are chosen in a different way.

Figure 25 schematically shows the unit cell with two ion cores and four BC, and the force interactions between the ions and BCs. The following notation is used: first, the quantities $\phi_{i1-i2}(t)$, $\phi_{i1-BC}(r_1)$, $\phi_{i2-BC}(r_2)$ describe a non-Coulomb elastic interaction of central type between the nearest adjacent ions and between the ions and BCs; secondly, the

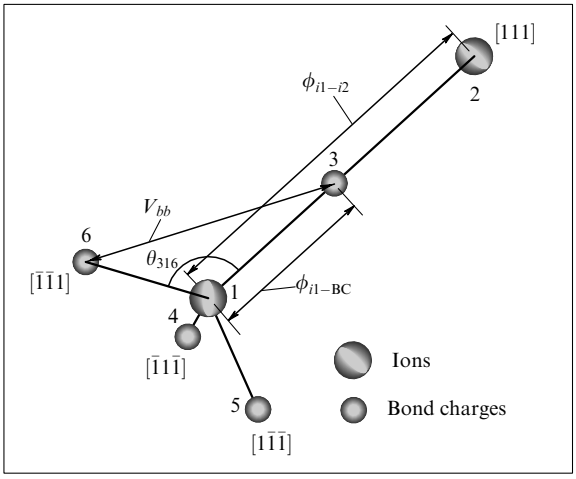

Figure 25. Structure of a unit cell and the interactions in the bond-charge model in the case of a homeovalent crystal [149].

quantity V_{bb}^{σ} defines the three-center interaction BC – ion – BC. It is described by a valence angle type coordinate. The superscripts $\sigma = 1$ and $\sigma = 2$ correspond to cations and anions, respectively.

It should be recognized that the part of the vibrational energy that is due to the short-range forces can be represented as a function of the so-called internal coordinates. Such coordinates account for the elongations of valence bonds, variations of valence angles, dihedral angles, etc. (see details in the description of models of valence-force type).

We denote the length of the interionic bond by t. Bond charges are localized at the points $r_1 = (1+p)t/2$, $r_2 = (1-p)t/2$. In this theory, for homeovalent crystals we have $p = 0$ $(r_1/r_2 = 1)$ (Fig. 25), and for III – V compounds and II – VI compounds we have, respectively, $p = 0.25$ $(r_1/r_2 = 5/3)$ and $p = 1/3$ $(r_1/r_2 = 2)$.

Let us reproduce the explicit expression for the three-center interaction potential V_{bb}^{σ} (see Fig. 25). Then we have

$$V_{bb}^{\sigma}(k,k') = \frac{B_{\sigma}}{8\,a_{\sigma}^2}\left[\mathbf{R}(\sigma k)\mathbf{R}(\sigma k') + a_{\sigma}^2\right]^2, \qquad (A.1)$$
$$\sigma = 1,2, \quad k,k' = 3,4,5,6.$$

Here, $\mathbf{R}(\sigma k)$ is the radius-vector of the kth BC, measured with respect to the ion core σ located at the vertex of an angle, and $a_{\sigma}^2 = -\mathbf{R}(\sigma k)\,\mathbf{R}(\sigma k')|_0$. The subscript $|_0$ indicates that the quantity is defined for the equilibrium configuration of particles.

The theory explicitly accounts for the interaction between BC. It is described by a central-type potential $\psi_{\sigma}(r_{bb}^{(\sigma)})$, where $r_{bb}^{(\sigma)}$ is the distance between BCs centered around a cation or an anion. In order to reduce the number of parameters, it is additionally assumed that

$$\psi_1' = \psi_2' = 0, \quad \psi_1'' = -\psi_2'' = \frac{B_2 - B_1}{8}, \qquad (A.2)$$

$$(1+p)\phi_{i1-BC}' + (1-p)\phi_{i2-BC}' = 0. \qquad (A.3)$$

Finally, the ions and BCs interact, as already said, with each other and between themselves through the long-range Coulomb forces. The particles have the charges $+2Ze$ and $-Ze$, so that the total charge of the unit cell is zero.

On the strength of the arguments developed above, the total energy of crystal lattice per unit cell can be written as

$$\Phi_{tot} = 4\left[\phi_{i1-i2}(t) + \phi_{i1-BC}(r_1) + \phi_{i2-BC}(r_2)\right] - \alpha_M\,\frac{(2Z)^2}{\epsilon}\,\frac{e^2}{t} + 6\left[V_{bb}^{(1)} + V_{bb}^{(2)} + \psi_1(r_{bb}^{(1)}) + \psi_2(r_{bb}^{(2)})\right]. \qquad (A.4)$$

Here α_M and ϵ are the Madelung constant and the dielectric constant, respectively.

The equation that governs the dynamic particle displacements $u_{\alpha}(\mathbf{n}k)$, located in the $\mathbf{n}$th cell of the lattice, can be represented in the standard form. We have

$$M_k\ddot{u}_{\alpha}(\mathbf{n}k) = -\frac{\partial\Phi_{tot}}{\partial u_{\alpha}(\mathbf{n}k)} = -\sum_{\mathbf{n}'k'\beta}\varphi_{\alpha\beta}(\mathbf{n}k,\mathbf{n}'k')u_{\beta}(\mathbf{n}'k'), \qquad (A.5)$$

where $\varphi_{\alpha\beta}(\mathbf{n}k,\mathbf{n}'k')$ are the force parameters, with

$$\varphi_{\alpha\beta}(\mathbf{n}k,\mathbf{n}'k') = \left.\frac{\partial^2\Phi_{tot}}{\partial R_{\alpha}(\mathbf{n}k)\partial R_{\beta}(\mathbf{n}'k')}\right|_0.$$

As said above, the numbers $k = 1, 2$ correspond to the cation and the anion, respectively. The numbers $k = 3, 4, 5, 6$ correspond to a BC with zero mass.

Now we rewrite equation (A.5) in the form

$$M_k\omega^2(\mathbf{q})u_{\alpha}(k) = \sum_{k'\beta}D_{\alpha\beta}(kk'\mathbf{q})u_{\beta}(k'). \qquad (A.6)$$

Here $D_{\alpha\beta}(kk'\mathbf{q})$ is an element of a Fourier component of the dynamic matrix.

In the expression for the D-matrix we distinctly separate the short-range and the long-range parts (D^{C}). Then we have

$$D_{\alpha\beta}(kk'\mathbf{q}) = \sum_{\mathbf{n}}\varphi_{\alpha\beta}(0k,\mathbf{n}k')\exp\left\{-i\mathbf{q}[\mathbf{R}(0k) - \mathbf{R}(\mathbf{n}k')\right] + D_{\alpha\beta}^{C}(kk'\mathbf{q}). \qquad (A.7)$$

The equations of motion (A.6) for the system of six particles (two ions and four BC) can be represented in the operator form as follows

$$\mathbf{M}\omega^2\tilde{\mathbf{u}} = \left[\mathbf{D}^{i-i} + 4\,\frac{(Ze)^2}{\epsilon}\mathbf{C}^{i-i}\right]\tilde{\mathbf{u}} + \left[\mathbf{D}^{i-BC} - 2\,\frac{(Ze)^2}{\epsilon}\mathbf{C}^{i-BC}\right]\mathbf{v}, \qquad (A.8)$$

$$\mathbf{0} = \left[\mathbf{D}^{i-BC,+} - 2\,\frac{(Ze)^2}{\epsilon}\mathbf{C}^{i-BC,+}\right]\tilde{\mathbf{u}} + \left[\mathbf{D}^{BC-BC} + \frac{(Ze)^2}{\epsilon}\mathbf{C}^{BC-BC}\right]\mathbf{v}. \qquad (A.9)$$

Here, $\tilde{\mathbf{u}}$ and $\mathbf{v}$ are the vectors of displacements of the ion cores and BCs, $\mathbf{M}$ is the matrix which defines the masses of ions. Matrices $\mathbf{D}^{i-i}$, $\mathbf{D}^{i-BC}$, and $\mathbf{D}^{BC-BC}$ are the dynamic matrices for the short-range ion – ion, ion – BC, and BC – BC interactions. Matrices $\mathbf{C}^{i-i}$, $\mathbf{C}^{i-BC}$, and $\mathbf{C}^{BC-BC}$ describe the Coulomb interaction that is calculated by the Ewald method.

The set of equations (A.8), (A.9) describing the dynamic displacements of the six particles consists of 18 equations. Since the BC species move adiabatically, these 18 equations

can be reduced to 6 equations which define the vibrational spectrum of ions in the crystal lattice. As a result, the frequencies and the polarization vectors are found as the solutions of the standard form of secular equation

$$|D_{ij}^{\text{eff}}(kk', \mathbf{q}) - M_k \omega(\mathbf{k})\, \delta_{ij}\, \delta_{kk'}| = 0, \quad k, k' = 1, 2\,. \text{ (A.10)}$$

The dynamic matrix D^{eff} in the last equation takes the following form

$$D^{\text{eff}} = D^{\text{i-i}} - [D]^{\text{i-BC},+} \left[D^{\text{BC-BC}}\right]^{(-1)} D^{\text{BC-i}}\,. \qquad \text{(A.11)}$$

Here, the first term describes the direct interaction between the ions, and the second accounts for the effects of BC on their motion.

Let us find the force parameters for the short-range forces. We take into consideration that for the case of pairwise central potentials $\phi_{\text{i1-i2}}(t)$, $\phi_{\text{i1-BC}}(r_1)$, and $\phi_{\text{i2-BC}}(r_2)$, we have by definition

$$\phi_{\alpha\beta}^{\text{cen}}(nk, n'k') = \frac{r_\alpha r_\beta}{r^2}\left[\phi'' - \frac{\phi'}{r}\right] + \delta_{\alpha\beta}\,\frac{\phi'}{r}\,, \qquad \text{(A.12)}$$

where $r = \left|\mathbf{R}(\mathbf{n}k) - \mathbf{R}(\mathbf{n}'k')\right|$. Concerning the three-center potential V_{bb}^{σ}, the corresponding contribution to the force parameters is found in the following manner. If one of the particles is an ion, and the other a BC, then one can write out the following relation

$$\phi_{ij}^{a}(lk, l'k') = \frac{B_\sigma}{4a_\sigma^2}\sum_{\tau=3}^{6} R_j(\sigma\tau)\left[R_i(\sigma k') + R_i(\sigma\tau)\right],$$

$$k = 1, 2, \quad k' = 3, 4, 5, 6\,. \qquad \text{(A.13)}$$

If both particles are BCs, then one obtains

$$\phi_{ij}^{a}(lk, l'k') = \frac{B_\sigma}{4\,a_\sigma^2}\, R_i(\sigma\, k')\, R_j(\sigma\, k), \quad k, k' = 3, 4, 5, 6\,. \qquad \text{(A.14)}$$

Next, in accordance with the condition of lattice equilibrium, we may write out

$$\frac{\partial \Phi}{\partial t} = 0\,, \qquad \text{(A.15)}$$

$$\frac{\partial \Phi}{\partial p} = 0\,. \qquad \text{(A.16)}$$

Using equality (A.15) and the definition (A.4) of the crystal energy per unit cell, we have

$$\phi'_{\text{i1-i2}} = -\alpha_{\text{M}}\,\frac{Z^2e^2}{2\epsilon t^2}\,. \qquad \text{(A.17)}$$

Using equality (A.16) and relation (A.3) we arrive at

$$\frac{\phi'_{\text{i1-BC}}}{r_1} = 2\,\frac{\mathrm{d}\alpha_{\text{M}}}{\mathrm{d}p}\,\frac{1-p}{1+p}\,\frac{Z^2e^2}{\epsilon t^3}\,, \qquad \text{(A.18)}$$

$$\frac{\phi'_{\text{i2-BC}}}{r_2} = -2\,\frac{\mathrm{d}\alpha_{\text{M}}}{\mathrm{d}p}\,\frac{1+p}{1-p}\,\frac{Z^2e^2}{\epsilon t^3}\,. \qquad \text{(A.19)}$$

In addition to Eqns (A.15) and (A.16), the inequalities $\partial^2\Phi/\partial t^2 > 0$, $\partial^2\Phi/\partial p^2 > 0$ must also hold in the case of a stable lattice. Using these inequalities and expression (A.3), we get the following two restrictions on the values of parameters:

$$4\,\frac{\phi''_{\text{i1-i2}}}{3} + (1+p)^2\left(\frac{\phi''_{\text{i1-BC}}}{3} + \frac{B_2}{6}\right) + (1-p)^2\left(\frac{\phi''_{\text{i2-BC}}}{3} + \frac{B_1}{6}\right) - \frac{128}{9\sqrt{3}}\,\alpha_{\text{M}}\,\frac{Z^2}{\epsilon} > 0\,, \qquad \text{(A.20)}$$

$$\frac{\phi''_1}{3} + \frac{\phi''_2}{3} + \frac{B_1 + B_2}{24} - \frac{64}{9\sqrt{3}}\,\frac{\mathrm{d}^2\alpha_{\text{M}}}{\mathrm{d}p^2}\,\frac{Z^2}{\epsilon} > 0\,. \qquad \text{(A.21)}$$

In this way, with the use of relations (A.17)–(A.19) and (A.2), we have defined the parameters ϕ'_{ii}, ϕ'_1, ϕ'_2, ψ'_1, ψ'_2, ψ''_1, and ψ''_2. Six parameters remain free in the theory, namely

$$\phi''_{\text{ii}}, \phi''_1, \phi''_2, B_1, B_2, \text{ and } \frac{Z^2}{\epsilon}\,.$$

For the homeopolar crystals, we have $\phi_{\text{i1-BC}} = \phi_{\text{i2-BC}}$ and $B_1 = B_2$, and the number of parameters reduces to four (the magnitude of the BC and three parameters for the non-Coulomb interactions). These parameters are found by fitting with the experimental neutron data and *elasticity moduli*.

Table 5 compiles the parameters of the theory for the elements of group IV of the Periodic System and III–V and II–VI compounds.

Table 5. Parameters of the bond-charge model for elements of group IV of the Periodic System and III–V and II–VI compounds. Force constants are expressed in units of e^2/Ω_0, where Ω_0 is the unit cell volume [150].

Element, compound	$\phi''_{\text{ii}}/3$	$\psi''_1/3$	$\psi''_2/3$	B_1	B_2	Z^2/ϵ	Z^+
Si	6.21	6.47	6.47	8.60	8.60	0.1800	1.47
Ge	6.61	5.71	5.71	8.40	8.40	0.1620	1.61
α-Sn	7.43	5.59	5.59	7.80	7.80	0.163	1.98
AlAs	5.80	2.27	15.48	5.79	8.54	0.1800	1.21
GaP	6.04	2.40	17.91	5.20	10.0	0.2030	1.36
GaAs	6.16	2.36	16.05	5.36	8.34	0.1870	1.43
GaSb	6.77	2.37	13.10	6.28	7.08	0.1600	1.52
InP	7.16	2.95	21.62	3.43	8.37	0.2490	1.55
InAs	7.31	2.64	17.86	3.99	7.30	0.2100	1.60
InSb	7.47	2.33	14.09	4.56	6.24	0.1720	1.64
ZnS	5.74	0.79	29.90	0.83	15.40	0.2130	1.05
ZnSe	5.01	1.19	22.82	1.21	15.65	0.1790	1.03
ZnTe	5.51	1.06	22.93	1.07	17.00	0.1800	1.05
CdTe	6.85	0.77	23.34	0.39	15.44	0.1830	1.15
HgSe	5.32	0.15	14.01	0.35	17.50	0.1095	0.91
HgTe	6.46	0.081	13.46	1.08	15.60	0.1062	1.03

References

1. De Bièvre P, Taylor P D P *Int. J. Mass Spectrom. Ion Proc.* **124** 149 (1993)
2. Ubbelohde A R *Trans. Faraday Soc.* **32** 525 (1936)
3. Robertson J M, Ubbelohde A R *Proc. R. Soc. London. Ser. A* **170** 222 (1939)
4. Maxwell E *Phys. Rev.* **78** 477 (1950)
5. Reynolds C A et al. *Phys. Rev.* **78** 487 (1950)
6. Geballe T H, Hull G W *Phys. Rev.* **110** 773 (1958)
7. Bardeen J, Cooper L N, Schrieffer J R *Phys. Rev.* **108** 1175 (1957)
8. Pomeranchuk I Ya *Zh. Eksp. Teor. Fiz.* **12** 245 (1942); see also *Sobranie Nauchnykh Trudov* (Collected Papers) Vol. 1 (Moscow: Nauka, 1972) pp. 122–142; *J. Phys. USSR* **6** 237 (1942)
9. Gel'd P V, Ryabov R A, Mokhracheva L P *Vodorod i Fizicheskie Svoĭstva Metallov i Splavov: Gidridy Perekhodnykh Metallov* (Hydrogen and Physical Properties of Metals and Alloys: Transition Metal Hydrides) (Moscow: Nauka, 1985)

10. Zhernov A P, Chernoplekov N A, Mrozan E *Metally s Nemagnitnymi Primesnymi Atomami* (Metals with Nonmagnetic Impurity Atoms) (Moscow: Energoatomizdat, 1992)
11. Richter D *Transport Mechanisms of Light Interstitials in Metal-Muon-Spin Rotation and Neutron Scattering* (Berlin: Springer-Verlag, 1983)
12. Kagan Yu M, Prokof'ev N V *Zh. Eksp. Teor. Fiz.* **90** 2176 (1986) [*Sov. Phys. JETP* **63** 1276 (1986)]
13. Vladár K, Zawadowski A *Phys. Rev. B* **28** 1564 (1983)
14. Vladár K, Zawadowski A *Phys. Rev. B* **28** 1582 (1983)
15. Vladár K, Zawadowski A *Phys. Rev. B* **28** 1596 (1983)
16. Trickey S B, Kirk W P, Adams E D *Rev. Mod. Phys.* **44** 668 (1972)
17. Esel'son B N et al. *Svoĭstva Zhidkogo i Tverdogo Geliya. Rastvory* ^{3}He – ^{4}He: *Spravochnik* (Properties of Liquid and Solid Helium. ^{3}He – ^{4}He solutions: Handbook) (Kiev: Naukova Dumka, 1982)
18. Ishmaev S N et al. *Zh. Eksp. Teor. Fiz.* **84** 394 (1983) [*Sov. Phys. JETP* **57** 228 (1983)]
19. Ishmaev S N et al. *Zh. Eksp. Teor. Fiz.* **89** 1249 (1985) [*Sov. Phys. JETP* **62** 721 (1985)]
20. Ishmaev S N et al. *Zh. Eksp. Teor. Fiz.* **102** 711 (1992) [*Sov. Phys. JETP* **75** 382 (1992)]
21. Bagatskiĭ M I et al. *Fiz. Nizk. Temp.* **12** 343 (1986)
22. Manzhelii V G *Can. J. Phys.* **65** 1471 (1987)
23. Korolyuk O A et al. *Fiz. Nizk. Temp.* **25** 944 (1999) [*Low Temp. Phys.* **25** 708 (1999)]
24. Gorodilov B Y et al. *J. Low Temp. Phys.* **119** 497 (2000)
25. Maradudin A A, Montroll E W, Weiss G H *Theory of Lattice Dynamics in the Harmonic Approximation* (New York: Acad. Press, 1963) [Translated into Russian (Moscow: Mir, 1965)]
26. Maradudin A A *Theoretical and Experimental Aspects of the Effects of Point Defects and Disorder on the Vibrations of Crystals* (New York: Acad. Press, 1966) [Translated into Russian: *Defekty i Kolebatel'nyĭ Spektr Kristallov* (Defects and Oscillation Spectrum of Crystals) (Moscow: Mir, 1968)]
27. Lifshitz I M, Kosevich A M *Rep. Prog. Phys.* **29** 217 (1966)
28. Lifshitz I M, Gredeskul S A, Pastur L A *Vvedenie v Teoriyu Neuporyadochennykh Sistem* (Introduction to the Theory of Disordered Systems) (Moscow: Nauka, 1982) [Translated into English (New York: Wiley, 1988)]
29. Kagan Yu M, in *Fizika Kristallov s Defektami: Materialy Shkoly po Teorii Defektov v Kristallakh i Radiatsionnykh Narusheniĭ, Telavi, Gruz. SSR, 1965* (Physics of Crystals with Defects: Materials of School on the Theory of Defects in Crystals and Radiation Disorders) Vol. 2 (Tbilisi: Izd. Inst. Fiz. AN Gruz. SSR, 1966) p. 93
30. Anthony T R et al. *Phys. Rev. B* **42** 1104 (1990)
31. Anthony T R, Banholzer W F *Diamond Relat. Mater.* **1** 717 (1992)
32. Itoh K et al. *J. Mater. Res.* **8** 1341 (1993)
33. Widulle F et al. *Physica B* **263 – 264** 381 (1999)
34. Takyu K et al. *Jpn. J. Appl. Phys. Pt. 2* **38** L1493 (1999)
35. Bulanov A D et al. *Cryst. Res. Technol.* **35** 1023 (2000)
36. Cardona M *Phys. Status Solidi B* **220** 5 (2000)
37. Vohra Y K, Vagarali S S *Appl. Phys. Lett.* **61** 2860 (1992)
38. Prigogine I, Bingen R, Jeener J *Physica* **20** 383 (1954)
39. Prigogine I, Jeener J *Physica* **20** 516 (1954)
40. Bättger H *Principles of the Theory of Lattice Dynamics* (Weinheim: Physik-Verlag, 1983)
41. Elliott R J, Krumhansl J A, Leath P L *Rev. Mod. Phys.* **46** 465 (1974)
42. Ehrenreich G, Schwartz L *The Electronic Structure of Alloys* (New York: Acad. Press, 1976) [Translated into Russian (Moscow: Mir, 1979)]
43. Rahman A et al. *Phys. Rev. B* **14** 3630 (1976)
44. Rafizadeh H A *Phys. Rev. B* **23** 1628 (1981)
45. Economou E N *Green's Functions in Quantum Physics* 2nd ed. (Berlin: Springer-Verlag, 1983)
46. Haydock R *Solid State Phys.* **35** 215 (1980)
47. Hass K C, Davis L C, Zunger A *Phys. Rev. B* **42** 3757 (1990)
48. Vast N, Baroni S *Phys. Rev. B* **61** 9387 (2000)
49. Born M, Kuhn H *Dynamical Theory of Crystal Lattices* (Oxford: The Clarendon Press, 1954) [Translated into Russian (Moscow: IIL, 1958)]
50. Leibfried G, Breuer N *Point Defects in Metals* (Berlin: Springer-Verlag, 1978)
51. Dirac P A M *The Principles of Quantum Mechanics* 4th ed. (Oxford: The Clarendon Press, 1958) [Translated into Russian (Moscow: Fizmatgiz, 1960)]
52. Landau L D, Lifshitz E M *Kvantovaya Mekhanika. Nerelyativistskaya Teoriya* (Quantum Mechanics. Non-Relativistic Theory) (Moscow: Nauka, 1974) [Translated into English (Oxford: Pergamon Press, 1977)]
53. Menéndez J, Page J B, Guha S *Philos. Mag. B* **70** 651 (1994)
54. Tamura S *Phys. Rev. B* **27** 858 (1983)
55. Tamura S *Phys. Rev. B* **30** 849 (1984)
56. Kunc K, Balkanski M, Nusimovici M A *Phys. Rev. B* **12** 4346 (1975)
57. Kunc K, Balkanski M, Nusimovici M A *Phys. Status Solidi B* **71** 341 (1975)
58. Kunc K, Balkanski M, Nusimovici M A *Phys. Status Solidi B* **72** 229 (1975)
59. Kunc K, Nielsen O H *Comput. Phys. Commun.* **16** 181 (1979)
60. Kunc K, Bilz H *Solid State Commun.* **19** 1027 (1976)
61. Borcherds P H, Kunc K *J. Phys. C* **11** 4145 (1978)
62. Kunc K, Nielsen O H *Comput. Phys. Commun.* **17** 413 (1979)
63. Cochran W *Philos. Mag.* **4** 1082 (1959)
64. Woods A D B, Cochran W, Brockhouse B N *Phys. Rev.* **119** 980 (1960)
65. Woods A D B et al. *Phys. Rev.* **131** 1025 (1963)
66. Cowley R A et al. *Phys. Rev.* **131** 1030 (1963)
67. Zhernov A P, Trenin A E *Fiz. Tverd. Tela* **27** 3543 (1985)
68. Zhernov A P, Trenin A E *Fiz. Met. Metalloved.* **66** 640 (1988)
69. Yanson I K, Khotkevich A V *Atlas Mikrokontaktnykh Spektrov Elektron-Fononnogo Vzaimodeĭstviya v Metallakh: Spravochnik* (Atlas of Microcontact Spectra of Electron-Phonon Interaction in Metals: Handbook) (Kiev: Naukova Dumka, 1986) [Translated into English: Khotkevich A V, Yanson I K *Atlas of Point Contact Spectra of Electron – Phonon Interactions in Metals* (Boston: Kluwer Acad., 1995)]
70. Yonezawa F, Odagaki T *Solid State Commun.* **27** 1199 (1978)
71. Odagaki T, Yonezawa F *Solid State Commun.* **27** 1203 (1978)
72. Yonezawa F, in *The Structure and Properties of Matter* (Springer Series in Solid-State Sciences, Vol. 28, Ed. T Matsubara) (Berlin: Springer-Verlag, 1982)
73. Göbel A et al. *Phys. Rev. B* **58** 10510 (1998)
74. Ho K-M, Fu C-L, Harmon B N *Phys. Rev. B* **28** 6687 (1983)
75. Sham L J *Phys. Rev.* **188** 1431 (1969)
76. Pick R M, Cohen M H, Martin R M *Phys. Rev. B* **1** 910 (1970)
77. Savrasov S Yu, Maksimov E G *Usp. Fiz. Nauk* **165** 773 (1995) [*Phys. Usp.* **38** 737 (1995)]
78. Martin R M *Phys. Rev.* **186** 871 (1969)
79. Hellmann H *Einführung in die Quantenchemie* (Leipzig: F. Deuticke, 1937)
80. Feynman R P *Phys. Rev.* **56** 340 (1939)
81. Gonze X, Vigneron J-P *Phys. Rev. B* **39** 13120 (1989)
82. Baroni S, Giannozzi P, Testa A *Phys. Rev. Lett.* **58** 1861 (1987)
83. Zeĭn N E *Fiz. Tverd. Tela* **26** 3028 (1984) [*Sov. Phys. Solid State* **26** 1825 (1984)]
84. Savrasov S Y *Phys. Rev. B* **54** 16470 (1996)
85. Wendel H, Martin R M *Phys. Rev. B* **19** 5251 (1979)
86. Kunc K, Martin R M *Phys. Rev. Lett.* **48** 406 (1982)
87. Yin M T, Cohen M L *Phys. Rev. B* **26** 3259 (1982)
88. Ihm J, Yin M T, Cohen M L *Solid State Commun.* **37** 491 (1981)
89. King-Smith R D, Needs R J *J. Phys.: Condens. Mat.* **2** 3431 (1990)
90. Giannozzi P et al. *Phys. Rev. B* **43** 7231 (1991)
91. Pavone P et al. *Phys. Rev. B* **48** 3156 (1993)
92. Kulda J et al. *Phys. Rev. B* **50** 13347 (1994)
93. Corso A D et al. *Phys. Rev. B* **47** 3588 (1993)
94. Parlinski K, Kawazoe Y *Phys. Rev. B* **60** 15511 (1999)
95. Karch K et al. *Phys. Rev. B* **50** 17054 (1994)
96. Wang C-Z, Yu R, Krakauer H *Phys. Rev. Lett.* **72** 368 (1994)
97. Lazarev A N, Mirgorodskiĭ A P, Smirnov M B *Kolebatel'nye Spektry i Dinamika Ionno-Kovalentnykh Kristallov* (Vibrational Spectra and Dynamics of Ion-Covalent Crystals) (Leningrad: Nauka, 1985)
98. Kvyatkovskiĭ O E, Maksimov E G *Usp. Fiz. Nauk* **154** 3 (1988) [*Sov. Phys. Usp.* **31** 1 (1988)]
99. Strauch D, Dorner B *J. Phys.: Condens. Mat.* **2** 1457 (1990)
100. Chrenko R M *J. Appl. Phys.* **63** 5873 (1988)

101. Hass K C et al. *Phys. Rev. B* **44** 12046 (1991)
102. Ramdas A K et al. *Phys. Rev. Lett.* **71** 189 (1993)
103. Ramdas A K, Rodriguez S *Phys. Status Solidi B* **215** 71 (1999)
104. Muinov M, Kanda H, Stishov S M *Phys. Rev. B* **50** 13860 (1994)
105. Fuchs H D et al. *Phys. Rev. B* **44** 8633 (1991)
106. Zhang J M et al. *Phys. Rev. B* **57** 1348 (1998)
107. Wang D T et al. *Phys. Rev. B* **56** 13167 (1997)
108. Widulle F et al. *Solid State Commun.* **118** 1 (2001)
109. Göbel A et al. *Phys. Rev. B* **56** 210 (1997)
110. Zhang J M et al. *Phys. Rev. B* **56** 14399 (1997)
111. Göbel A et al. *Phys. Rev. B* **59** 2749 (1999)
112. Widulle F et al. *Phys. Rev. Lett.* **82** 3089 (1999)
113. Widulle F et al. *Phys. Rev. Lett.* **82** 5281 (1999)
114. Widulle F et al. *Phys. Status Solidi B* **215** 131 (1999)
115. Balkanski M, Wallis R F, Haro E *Phys. Rev. B* **28** 1928 (1983)
116. Cardona M, Ruf T *Solid State Commun.* **117** 201 (2001)
117. Fuchs H D et al. *Phys. Rev. Lett.* **70** 1715 (1993)
118. Debernardi A, Baroni S, Molinari E *Phys. Rev. Lett.* **75** 1819 (1995)
119. Hass K C et al. *Phys. Rev. B* **45** 7171 (1992)
120. Vogelgesang R et al. *Phys. Rev. B* **54** 3989 (1996)
121. Spitzer J et al. *Solid State Commun.* **88** 509 (1993)
122. Vast N, Baroni S *Comput. Mater. Sci.* **17** 395 (2000)
123. Ruf T et al. *Solid State Commun.* **105** 311 (1998)
124. Timofeev Yu A, Vinogradov B V, Stishov S M *Pis'ma Zh. Eksp. Teor. Fiz.* **69** 211 (1999) [*JETP Lett.* **69** 227 (1999)]
125. Vogelgesang R et al. *Phys. Rev. B* **58** 5408 (1998)
126. Rohmfeld S et al. *Phys. Rev. Lett.* **86** 826 (2001)
127. Klemens P G, Maradudin A A *Phys. Rev.* **123** 804 (1961)
128. Glyde H R *Phys. Rev.* **177** 262 (1969)
129. Jones H D *Phys. Lett. A* **1** 71 (1970)
130. Zhernov A P *Zh. Eksp. Teor. Fiz.* **114** 2153 (1998) [*JETP* **87** 1172 (1998)]
131. Verkhovskii S V et al. *Appl. Magn. Reson.* **17** 557 (1999)
132. Verkhovskii S V et al. *Z. Naturforsch. A* **55** 105 (2000)
133. Leibfried G, Ludwig W *Theory of Anharmonic Effects in Crystals* (New York: Acad. Press, 1961) [Translated into Russian (Moscow: IIL, 1963)]
134. Krivoglaz M A *Fiz. Met. Metalloved.* **10** 169 (1960)
135. Soma T *Physica B* **92** 1 (1977)
136. Solt G *Phys. Rev. B* **18** 720 (1978)
137. Zhernov A P, Mamedov T A *Phys. Status Solidi B* **103** 477 (1981)
138. Zhernov A P *Fiz. Nizk. Temp.* **26** 1226 (2000) [*Low Temp. Phys.* **26** 908 (2000)]
139. Solt G, Zhernov A P *J. Phys. F* **9** 1013 (1979)
140. Wagner H, Horner H *Adv. Phys.* **23** 587 (1974)
141. Yakubovskiĭ A et al., Private communication (2001)
142. Stoneham A M *Rev. Mod. Phys.* **41** 82 (1969)
143. Mehring M, Kanert O, in *Progress of Magnetic Resonance Spectroscopy* Vol. 3 (Berlin: Springer-Verlag, 1972)
144. Ivanov M A et al. *J. Magn. Magn. Mater.* **36** 26 (1983)
145. Maradudin A A, Ganesan S, Burstein E *Phys. Rev.* **163** 882 (1967)
146. Ham F S, in *Electron Paramagnetic Resonance* (Ed. S Geschwind) (New York: Plenum Press, 1972)
147. Weber W *Phys. Rev. Lett.* **33** 371 (1974)
148. Weber W *Phys. Rev. B* **15** 4789 (1977)
149. Eryiğit R, Herman I P *Phys. Rev. B* **53** 7775 (1996)
150. Rajput B D, Browne D A *Phys. Rev. B* **53** 9052 (1996)